Flux Kinetics, Limit and Critical Fluxes for Low Pressure Dead-end Microfiltration. The case of BSA Filtration through a Positively Charged Membrane

C. Velasco, J.I. Calvo, Laura Palacio, Javier Carmona, Pedro Prádanos and A. Hernández*

Group of Surfaces and Porous Materials UA UVA-CSIC, Dpto. de Física Aplicada, Paseo de Belén, Facultad de Ciencias Universidad de Valladolid, 47071 Valladolid, Spain.

ABSTRACT

The influence of the applied pressure on the flux decay mechanism during Bovine Serum Albumin (BSA) dead-end microfiltration (MF) has been investigated for a polyethersulfone, positively charged, membrane (SB-6407®) from Pall®. BSA solutions, at pH values of 4, 5 (very close to the protein isoelectric point, IEP) and 6, were micro-filtered through the membrane at different low applied transmembrane pressures.

Although filtration was done in dead-end configuration, limit fluxes appeared for all pressures and pH values studied. The concepts of (long time) limit and critical fluxes and their correlation have been clarified and analysed too. The usual blocking filtration laws have been included in a common frame and both the cases with zero or non-zero limit fluxes have been incorporated. Within this frame, the standard model, that assumes an internal pore deposition, has been included as well; although, in our case, the acting mechanism seems to be mainly the so called complete blocking.

Protein adsorption has been analysed in terms of the protein-protein and protein-membrane electrostatic interactions. There is a faster flux-decay for the protein isoelectric point with a slightly slower decline in flux when there are both membrane-to-protein and protein-protein repulsion. The slowest kinetics appears for membrane-to-protein attraction with protein-protein repulsion. Moreover, adsorption is stronger, and the limit flux smaller, when the protein is attracted towards the membrane and there is protein-protein repulsion.

KEYWORDS

Proteins, Dead-end Microfiltration, Flux decay kinetics, Limit and Critical fluxes, Adsorption.

(*) To whom correspondence should be addressed.
Group of Surfaces and Porous Materials UA UVA-CSIC, Dpto. de Física Aplicada, Paseo de Belén s/n,
Facultad de Ciencias, Universidad de Valladolid, 47071 Valladolid, Spain.
Phone: +34-983423134. Fax: +34-983423013. E-mail: tonhg@termo.uva.es

1. Introduction.

Membrane microfiltration is a well-established procedure in biotechnological and biochemical industries, **[*1-4*]**. Microfiltration membranes are especially adequate for the separation of fine particles with sizes in the range from 0.1 to 10.0 microns, especially in cell recovery from fermentation broths, polishing and sterilization of product solutions. It is also used to separate cell fragments caused by cell disruption for the recovery of intracellular enzymes.

Protein transmission and the rate of filtration during microfiltration of protein solutions has been extensively studied and reviewed, **[5-*9*]**. In fact, the transmission of proteins through microfiltration membranes is usually high. Even so, the rate of filtration of apparently pure protein solutions decreases with time at a constant applied pressure. In some cases, this has been explained in terms of deposition of protein in the front face of the membrane, **[*6*]**. It has also been shown that in such cases the adsorption of protein (BSA) is associated with the deposition of trace quantities of aggregated and/or denaturated protein that act as initiators for the continued deposition of bulk protein, **[*6,7*]**. However, a continuous decrease in filtration rate has also been reported in cases where there is neither deposition nor concentration polarization on the front face of the membrane, **[8,*10-12*]**.

Usually less attention than would be required has been devoted to the applied pressure used to measure the flux decrease linked to pore narrowing or clogging due to adsorption or deposition. A notable exception is the work of Grenier et al., [13], where an extensive analysis of the pressure dependence of deposition parameters is performed in dead-end microfiltration of bentonite suspensions that don't show a non-zero limit flux. In any case, the convenience of a reduction of the operating pressure to decrease pore blocking was already recommended by Bowen et al., [***14***].

The origin of limit fluxes – those reached in stationary conditions after long enough times—is not well understood. It is worth noting that in some texts, the more or less pressure independent fluxes reached after applying high enough pressures have been also called limit fluxes, [***15***]. Here, we will only use "limit fluxes" to refer to the long time stationary flux reached at each constant pressure. The cause of critical fluxes, those appearing for relatively high pressures with a decrease in permeability, is neither well identified nor understood. It is clear, that when there is a high pressure flux plateau with a very low permeability, this critical flux can be attributed to an extreme blockage of pores. We will further discuss the conceptual differences and the correlation of limit and critical fluxes below. Nevertheless, we will not refer here to other conceptually different critical fluxes as, for example, those corresponding to the maximum flux before arriving to an irreversible fouling, [***16-19***].

Limit fluxes were originally attributed to factors like cake erosion or deposit removal or back flux, [***20***]. Actually the introduction or quantification of these limit fluxes has been, from the very beginning, substantially phenomenological, [***21-23***]. Though the limit fluxes were originally introduced for cross-flow microfiltration, they can also appear in dead end microfiltration, [***24, 25***]. Although, of course, the sweeping action of tangential

flow would cause the partial loss of the deposit, other causes, as for example the equilibrium between pressure and the attraction or repulsion between the membrane and the solute or the solute-solute interaction, can play a similar role, by limiting the extension and compactness of the deposit. It seems clear that these subtle balances would be more plausible for low pressures because high pressures would always overcome any other interaction. An extensive review of the different theoretical and experimental methodologies applied to cross-flow and dead-end limit and critical fluxes was presented by Bacchin, Aimar and Field, [16].

In any case, as pointed out by Franken, [***26***], present day micro- and ultrafiltration (as well) equipment is designed and operated with a strong accent on avoiding the rise of membrane resistance. Nearly all membrane installations in water treatment are using a very low transmembrane pressure. Whatever way the phenomenon is described (critical flux, limit flux, low pressure), it all comes down to keep the overall resistance as low as possible. In practice this, however, can lead to very low fluxes and/or to the requirement of huge membrane surfaces, this is why the question on what pressures can be applied to avoid an inconvenient increase of the membrane resistances while keeping the needed membrane within reasonable limits is relevant.

Our aim here is to study how the applied pressure intensity can affect both the intensity and kinetics of flux decay or fouling due to deposition. This for a charged membrane should depend on the solution pH and on the details of the membrane charge. The influence of pH in dead end microfiltration of proteins has been previously addressed by us using BSA and Lysozyme and positive, SB-6407®, and negative membranes, ICE-450®, [***27***], for a relatively high pressure. The influence of pressure for BSA microfiltration was also analyzed, [***28***], with the negatively charged membrane, ICE-450®. In all these cases, the fouling kinetics was clearly faster for high pressures although limit fluxes were always very small and could be considered zero without affecting substantially retention that remained insignificant. Here we will use the positive SB-6407® membrane to microfilter BSA at low pressures and different pH values. We will find non-zero limit fluxes for all pressures and pH and we will analyze the intensity and kinetics of flux decay in terms of both membrane-solute and solute-solute electrostatic interactions.

2. Theory.

2.1. Flux Decay Mechanisms

Usually, the kinetics of flux decline is analysed in terms of different blocking laws which are customarily four, namely: standard blocking, intermediate blocking, cake filtration and complete blocking models, [***29-32***]. In the first of these models, the standard model, it is assumed that the solute molecules or particles are adsorbed onto the walls of the pores decreasing their effective radii. The other three models assume that deposition happens externally. In the complete blocking model each molecule or aggregate (or particle) is assumed to obstruct a pore. In the intermediate model some of the pores clog up while some molecules attach to external non-porous surfaces or on other pre-existent deposits. Finally, in the cake filtration model, a cake can form on the membrane.

For all of these mechanisms, it has been shown, [***29-32***], that there is a common simple characteristic equation:

$$\frac{d^2t}{dV^2} = \alpha\left(\frac{dt}{dV}\right)^{\beta} \quad \textbf{(1)}$$

The physical meanings of the parameters of the four usual models, constants α and β, are well known, **[*29-32*],** and are shown in Table I.

Table I.- Values of : α , β, α', γ, ($\gamma\alpha$') and n for the different blocking mechanisms.

The meaning of the constants involved in α is:

- K_A is the membrane surface blocked per unit of total volume permeated through the membrane
- K_B is the decrease in the cross section area of the pores (due to adsorption on the pore walls) per unit of total permeated volume
- $1/K_C$ is the total permeate volume per unit of membrane area (i.e. per unit of the deposited cake area)
- R_r is the ratio of the hydraulic resistance of the cake to the initial or clean membrane resistance, ($R_r = R_C/R_0$)
- A_0 is the porous surface of the membrane and,
- u_0 is the mean initial velocity of the filtrate.

According to the definition of the permeate flux as $J_V = dV/dt$, Equation (1) can be written as:

$$-\frac{dJ_V}{dt} = \alpha J_V^{3-\beta} \quad \textbf{(2)}$$

This relationship simplifies the process of fitting of the experimental data to obtain the corresponding blocking parameter, β.

If the flux per unit area, $J = J_V / A_m$, is used, Equation (2) reads:

$$-\frac{dJ}{dt} = \alpha' J^{3-\beta}$$
$$\alpha' = \alpha\left(\frac{A_m^2}{A_m^{\beta}}\right) \quad \textbf{(3)}$$

The values of α' are shown in Table I. Note that:

$$J(t=0)=J_0=\frac{J_{V0}}{A_m}$$
$$u_0 = \frac{J_{V0}}{A_0} \quad \textbf{(4)}$$
$$\Theta = \frac{A_0}{A_m}$$

A_0 is the porous transversal area of the membrane and Θ is the surface porosity.

2.2. *Limit Flux*

We can define the limit flux for a given pressure, as the stable flux that is achieved once flux decline ceases for a constant pressure experiment As mentioned, in some cases a limit flux, for long times, appears:

$$J^* = \lim_{t\to\infty} J = \lim_{t\to\infty}\left(\frac{J_V}{A_m}\right) \quad \textbf{(5)}$$

This is common, for example, in cross flow filtration.

Field et al., [***20, 33, 34***], performed some modifications in the models of Hermia, in order to include the possible existence of a J*, for: complete, intermediate and cake mechanisms. The limit flux appeared there linked to the partial removal of the substances deposited on the membrane caused by the tangential flow. As a consequence they transformed Equation (3) to:

$$-\frac{dJ}{dt}J^{\beta-2} = \alpha'\left(J - J^*\right) \quad \textbf{(6)}$$

The constant in the right hand term must be equal to α' in order to recover Equation (3) when J*=0. Of course this is equivalent to:

$$-\frac{dJ_V}{dt}J_V^{\beta-2} = \alpha\left(J_V - J^*_V\right) \quad \textbf{(7)}$$

with $J^*_V = J^*A_m$. This equation can be written in terms of derivatives of time as:

$$\frac{d^2t}{dV^2} - \alpha\left(\frac{dt}{dV}\right)^{\beta} + \alpha J^*_V\left(\frac{dt}{dV}\right)^{\beta+1} = 0 \quad \textbf{(8)}$$

or

$$\frac{d^2t}{dV^2} = \alpha\left[1 - \frac{J^*_V}{J_V}\right]\left(\frac{dt}{dV}\right)^{\beta} \quad \textbf{(9)}$$

Of course, Equation (1) is recovered from Equations (8) or (9) when $J^*_V=0$.

Equation (6) can be rearranged to:

$$\frac{dJ}{dt} = -\alpha'\left(J - J^*\right)J^{2-\beta} \quad \textbf{(10)}$$

or

$$\int \frac{J^{\beta-2}}{J - J^*}dJ = A - \alpha' t \quad \textbf{(11)}$$

with A being a constant of integration. Equation (10) should be adequately integrated.

It can be integrated for the cake fouling i.e. for β =0 [β-2 = -2] to:

$$\frac{J\ln\left(J - J^*\right) - J\ln J + J^*}{JJ^{*2}} = A - \alpha' t \quad \textbf{(12)}$$

The integration for the intermediate fouling i.e. for β =1 [β-2 = -1] leads to:

$$J = \frac{J^* e^{\alpha' J^* t}}{e^{\alpha' J^* t} + J^* A} \quad \textbf{(13)}$$

For standard fouling with β =3/2 [β -2=-1/2]:

$$\left(\frac{1}{\sqrt{J^*}}\right)\ln\left(\frac{\sqrt{J}-\sqrt{J^*}}{\sqrt{J}+\sqrt{J^*}}\right) = A - \alpha' t \quad \textbf{(14)}$$

that could be used by assuming that a limit flux could exist also for the standard fouling, which was not assumed by Field because tangential flow wouldn't lead to any removal of the material deposited inside the pores, although for wide enough pores convection would cause enough shear to act in a similar way. In dead-end filtration especially, convection through the pores could certainly be crucial to reach equilibrium between deposition and removal due to the shear stress introduced along the pore. Other factors can also imply a limit on the increase of adsorption or deposition.

Finally, for the complete blocking for β=2 (β-2=0):

$$J = Ae^{-\alpha' t} + J^* \quad \textbf{(15)}$$

Equation (15), by recalling that $J(t=0)=J_0=J_{V0}/A_m$, gives:

$$\frac{J}{J_0} = \left(1 - \frac{J^*}{J_0}\right)e^{-\alpha' t} + \frac{J^*}{J_0} \quad \textbf{(16)}$$

because $A = J_0 - J^*$ for the complete blocking mechanism. Equivalently, Equations (12), (13) and (14) can be written in terms of J_0 as shown in the next section. It is worth mentioning that Field and Wu [34] re-evaluated the flux versus time relationship for the complete blocking mechanism and concluded that shear stress couldn't explain a non-zero limit flux when removal terms for cross flow could be considered both linearly dependent upon shear stress or proportional to shear stress and inversely proportional to flux, in addition to be proportional to the blocked area. Even in these cases, Equation (16) can be written in the same form, although Field and Wu preferred to avoid naming the long time flux as J* because this limit flux could'nt be ~~not be assigned to~~ due to the shear appearing in cross flow filtration.

2.3. Time Dependence of Flux

It is worth noting that Equations (12-14), lead to 0/0 indeterminations for J*=0. While Equation (15) leads to:

$$J = J_0 e^{-\alpha' t} \quad \textbf{(17)}$$

that could be obtained as well from Equation (3). For the intermediate mechanism:

$$A = \frac{1}{J_0} - \frac{1}{J^*} \quad \textbf{(18)}$$

and applying L'Hopital, the equation for the J versus time dependence for J*=0 is:

$$\frac{J}{J_0} = \frac{1}{\left(1 + J_0 \alpha' t\right)} \quad \textbf{(19)}$$

according to the corresponding result from Equation (3) directly. Similarly, for the standard fouling case:

$$A = \left(\frac{1}{\sqrt{J^*}}\right)\ln\left(\frac{\sqrt{J_0}-\sqrt{J^*}}{\sqrt{J_0}+\sqrt{J^*}}\right) \quad \textbf{(20)}$$

and applying L'Hopital:

$$\frac{J}{J_0} = \frac{1}{\left(1+\frac{\alpha'\sqrt{J_0}}{2}t\right)^2} \quad \textbf{(21)}$$

for J*=0 in accordance again with the corresponding result from Equation (3). Finally for the cake mechanism

$$A = \frac{J\ln\left(J_0 - J^*\right) - J_0 \ln J_0 + J^*}{J_0 J^{*2}} \quad \textbf{(22)}$$

and after application of the L'Hopital rule twice:

$$\frac{J}{J_0} = \frac{1}{\left(1+2\alpha' J_0^2 t\right)^{1/2}} \quad \textbf{(23)}$$

for J*=0, that is once again in agreement with the solution from Equation (3).

Equations (19), (21) and (23) can be written as:

$$\frac{J}{J_0} = \frac{1}{\left(1+\gamma\alpha' t\right)^n} \quad \textbf{(24)}$$

The values of γ , n and $\gamma\alpha$' are shown in Table I.

2.4. General Time Dependence of Flux

In general the integral in Equation (11) will be called here integral filtration coefficient:

$$\Lambda \equiv \int \frac{J^{\beta-2}}{J - J^*} dJ \quad \textbf{(25)}$$

or

$$\Lambda \equiv \int J^{\beta-3} dJ \quad \textbf{(26)}$$

for J*=0.

Therefore, equation (11) would read as:

$$\Lambda = A - \alpha' t$$

$$A = \Lambda_0 \quad \textbf{(27)}$$

$$\alpha' = -\frac{d\Lambda}{dt}$$

This gives a meaning for - Λ as:

$$-\Lambda(t) = \int_{o}^{t} \alpha'(t)\, dt \qquad (28)$$

and of course depends on the meaning for α' for each flux decay mechanism shown in Table I.

It is worth noting that given that the integral filtration coefficient would be linear with t (if α' does not depend on time, as usually assumed for each fouling mechanism) it is easy to test, by using this coefficient, what mechanism is followed. Of course the lack of linearity could be attributed to the presence of a time depending α' as would be the case if a mixture or sequence of several mechanisms were assumed.

2.4. Critical Flux

Field et al. in the seminal paper of 1995 introduced the concept of "critical flux" in membrane technology, [***20, 33***]. It defines a critical value of the permeate flux below which no flux decay would occur. The critical flux should depend on: hydrodynamic forces, transmembrane pressure, electrostatic interaction between feed components and with the membrane surface, etc. Even though it is accepted that low-pressure microfiltration is much more effective than high-pressure microfiltration, the emphasis in the concept of critical flux is that it should be appropriate to start filtration operations at a low flux and increase it until reaching the critical value and this could be done without any, or with a controlled low, decline of flux with time [***20***]. In this way a window of operation should be used where "the membrane resistance remains constant as the flux is increased and thus there is a linear relationship between flux and transmembrane pressure" in words of Franken **[*26*]**.

This also resulted in the definition of a "strong form of critical flux" and a "weak form of critical flux". In the first definition a "strong form" of critical flux, it is reached when flux is not anymore identical to the flux of clean water at the same transmembrane pressure but the slope of the line (and the permeability) is lower than that of the initially clean membrane, [***33***]. In the second definition a "weak form" of the critical flux is reached when the linear relationship between transmembrane pressure and flux ceases. It is worth considering that the "strong concept" critical flux happens when fouling is still low but fast while "weak concept" critical flux is associated with high levels of slow fouling.

The concept of critical flux is different from the limit flux appearing in the preceding sections. It seems clear that, according to Equation (6), the flux doesn't decrease when J=J*, but also that when J<J* the flux should increase, although Field [***20, 33***] included the caveat that dJ/dt =0 for $J_0 \leq J^*$. Of course an increase of the flux would be unreasonable. Actually, the dependence of J* on the applied constant pressure (for a given solution-membrane system) should prevent this to happen because if we started with a reduced pressure in order to have low J, the corresponding J* would also be reduced. Thus it should be always $J_0 \geq J^*$ and because, according again with Equation (6), the time evolution of J with time must be monotonous, this should ensure that J>J* (if J_0 >J*) and that J should decrease always or be J=J* constantly (if J_0=J*).

Another question should be: is there a minimum J_0 (with J>J*), below which J*=J_0 always? If this minimum J_0 (or J*) exists it could be called critical flux J_{1c}. This should correspond to the called "strong form" of critical flux if we assume that J_0 versus △p plot corresponds to that for pure water because initial deposition could not have happened yet. If there were a maximum J* that should be reached from any initial flux J_0 this critical flux should correspond to a "weak form" of critical flux, J_{2c}. In Figure 1 the critical fluxes (strong and weak concepts) are shown schematically in terms of the steady state fluxes J*, and the ΔJ*/Δp gradients, as a function of constant applied pressure. According to Bacchin [***15***], there is a limiting flux corresponding to the flux that can't be surpassed at any pressure, no matter how high it could be, that should be $J_{3c}=3J_{2c}/2$. As mentioned we don't deal with this high pressure limiting flux here.

Figure 1.- Critical and limit fluxes and steady state flux versus pressure gradients. Actually, the steps in the gradients would be more gradual.

2.5. Zeta potentials and Membrane Charge Density

In order to understand the changes in fouling and flux decay kinetics with pH it is useful to think in terms of the membrane-protein and protein-protein interactions that can be interpreted approximately in terms of their (membrane and protein) electrical properties alone. Here we will focus on the electrostatic interaction although it is well known that short range forces play a key role especially near the zero charge conditions (isoelectric point). In this and the next sections, we will pay special attention to the charge of the membrane, while the charge of BSA will be taken from literature (as shown below in Figure 5-a).

It has been shown that, to obtain accurate estimations of zeta potentials, and especially to evaluate the isoelectric point of a membrane, the streaming potential can be measured on or through the membrane [***35***] for an aqueous solution of a salt. When the pores are very narrow, diffusion potentials should appear due to retention and the solution of the Poisson-Boltzmann equation inside the pores can be difficult. Also the shape and tortuosity may be relevant for narrow pores. Nevertheless, for wide-enough pores the treatment of the streaming potential through the pores is easy and this procedure should be preferable because it refers to the actual transport path. No significant differences appear within the streaming potential on and through the membrane when any differences between the surface and inner materials could be expected.

In a steady Poiseuille flow through a capillary channel, a relationship between the streaming potential coefficient (ratio of potential difference △E to the applied pressure gradient △p) and the zeta potential ζ, is described by:

$$\nu_p \equiv \frac{\Delta E}{\Delta p} = \frac{\varepsilon \zeta}{\eta\left(\lambda_0 + \frac{\lambda_s}{r_p}\right)} \qquad \textbf{(29)}$$

Equation (29) is the well-known Helmholtz–Smoluchowski equation. In this equation, the specific surface conductivity λ_s is taken into account along with the electrolyte conductivity λ_0. ε is the dielectric constant, η the viscosity of the electrolyte solution, and r_p the capillary radius. Assuming that the dielectric constant of the solution is very large as compared to that of the membrane material, λ_s / r_p can be neglected in the Helmholtz–Smoluchowski equation, then:

$$\zeta = \nu_p \frac{\mu \lambda_0}{\varepsilon} \tag{30}$$

The charge density on the membrane surface can be obtained by, [***36***]:

$$\sigma = \frac{2\varepsilon RT}{F\kappa^{-1}} \sinh \frac{\bar{\zeta}}{2} \tag{31}$$

Here $\bar{\zeta}$ is the dimensionless zeta potential:

$$\bar{\zeta} = \frac{F\zeta}{2RT} \tag{32}$$

R is the gas constant, T the temperature and F the Faraday constant. Finally κ^{-1} is the Debye's length.

Therefore, by this procedure, the surface charge density on the membrane can be obtained from streaming potential measurements, once the zeta potential has been obtained from Equation (30) and the Debye's length is known. The charge number density (per unit of membrane area) is then easily obtained as $Z/A = \sigma / |e|$ where *e* is the elemental charge.

2.6. Ionic Strength and Debye's Length.

As a consequence of the colloidal behavior of the protein molecules at different pH in an aqueous solution, they are surrounded by an electrical double layer with a thickness given by the Debye's length that can be evaluated according to:

$$\kappa^{-1} = \sqrt{\frac{\varepsilon RT}{F^2 \sum_i z_i^2 c_i}} \tag{33}$$

Here, z_i is the charge number of the i-th charged species in the solution and c_i is its concentration. This expression can be simplified by substitution to:

$$\kappa^{-1} = \frac{0.3041}{\sqrt{I}} \tag{34}$$

This gives the Debye's length in nanometers with the ionic strength:

$$I = \frac{1}{2} \sum_i z_i^2 c_i \tag{35}$$

in mol/L.

3. Experimental.

3.1. Membranes and Chemicals.

We used here polymeric microfiltration membranes, obtained from Pall Co®, consisting in flat disks of 47 mm in diameter. Their pore size is 0.45 μm and they have an anion exchange character. The membranes are called SB-6407® by the manufacturer and consist in polyethersulfone unsupported filters that are strongly positively charged by a patented post-treatment process. Other nominal characteristics of these filters are shown in Table II.

Table II.- Nominal characteristics of the filters used.

Bovine serum albumin (BSA) was obtained from Sigma Aldrich (product no. A-6793). 1 g of BSA was dissolved in 1 L of a buffer solution, consisting in a 0.06 mol/L aqueous solution of pure orthophosphoric acid. pH of the resulting solution was adjusted to 4.0, 5.0 and 6.0 (± 0.1) by stepwise addition of drops of a NaOH concentrated solution. Aqueous solutions $1 \cdot 10^{-3}$ mol/L of KCl from Fluka were used for the streaming potential measurements.

All chemicals were of analytical grade and the water used to prepare the solutions was bidistilled and then Milli-Q treated to be almost free of dissolved ions. Solutions were afterwards kept refrigerated for 6 hours before being used. Then pH was readjusted if necessary.

3.2 Filtration Setup.

Dead-end filtration was performed at constant temperature (295 ± 1 K), in a simple device described elsewhere, **[*31, 37*]**, which allows to maintain a constant applied pressure by a liquid column. The permeated flux is measured by a microbalance connected to a PC computer. The applied pressure was kept constant in the range from 1000 to 7000 ± 10 Pa. It is important to point out that because pressure is applied by using a liquid column, pumping denaturation is prevented. In all cases a totally negligible retention was measured.

3.3 Streaming Potential.

The streaming potential experiments were conducted for relatively high concentrations of KCl as mentioned in section 3.1. KCl, among simple salts, has very similar and high mobility for both the anions and cations, **[*38*]**. The through-the-pores streaming potential (ν_p) measurements were performed by us [***27***] with the experimental device described elsewhere, **[*37*].**

In order to evaluate the ionic strength and the corresponding Debye`s length the dissociation equilibria of the buffer 0.06 mol/L solution of orthophosphoric acid, used to control the different pH, have to be taken into account. The three following equilibria appear. Firstly:

$$H_3PO_4 + H_2O \Leftrightarrow H_2PO_4^- + H_3O^+ \quad \textbf{(36)}$$

$$K_1 = \frac{\left[H_2PO_4^- \right]\left[H_3O^+ \right]}{\left[H_3PO_4 \right]} \quad \textbf{(37)}$$

that predominates for pH lower than 7 with k_1=7,5.10^{-3}. For pH between 7 and 12 the main equilibrium is:

$$H_2PO_4^- + H_2O \Leftrightarrow HPO_4^{-2} + H_3O^+ \quad \textbf{(38)}$$

$$K_2 = \frac{\left[HPO_4^{-2} \right]\left[H_3O^+ \right]}{\left[H_2PO_4^- \right]} \quad \textbf{(39)}$$

with K_2 = 2.10^{-7}. Finally over pH 12 the prevailing equilibrium is:

$$H\,PO_4^{-2} + H_2O \Leftrightarrow PO_4^{-3} + H_3O^+ \quad \textbf{(40)}$$

$$K_3 = \frac{\left[PO_4^{-3} \right]\left[H_3O^+ \right]}{\left[HPO_4^{-2} \right]} \quad \textbf{(41)}$$

with a constant K_3 = 10^{-12}.

The corresponding values for I, obtained from Equations (37), (39) and (41), and κ^{-1} are shown in Table III.

Table III.- Ionic Strength and Debye's length for water solution of orthophosphoric (H_3PO_4) acid as a function of pH.

4. Results and Discussion.

Figure 2 shows an example of the flux decay (for pH=6 and Δp= 4.85 KPa) showing how a clear limit flux is reached – in this case after 2 hours of filtration. As already mentioned, although frequently limit fluxes aren't

found for dead end filtration, nothing fundamental forbids the appearance of this phenomenon in any filtration mode provided that there is a mechanism that can avoid indefinite fouling [16].

Figure 2.- Flux decay for pH=6 and Δp= 4.85 KPa. The gray line corresponds to the complete fouling model.

The corresponding limit fluxes are shown in Figure 3, along with the initial ones, for the different pH values studied here. It seems clear that fouling increases for increasing pH, in terms of a clear decrease of J*. Note that the initial flux is very approximately equal for all pH values as should correspond to the pure non fouling permeation. Small differences could be attributed to the ambiguities in a correct identification of the zero-time flux, although at the isoelectric point there is a slightly higher initial flux that could be due to a delay in the time of arrival to the membrane of the large aggregates. The identity of pure pure-water fluxes and the initial fluxes were confirmed, within the error range, by measuring those for all pH and pressures used here.

The critical flux corresponding to the maximal flux with no decrease of resistance – "strong concept" critical flux, which is marked with a square, ⌖, in Figure 3 –, decreases with increasing pH to be essentially zero at pH 6. On the other hand, the "weak concept" critical flux, marked as ⌖ in Figure 3, that corresponds to the maximum flux with constant resistance (but lower than that in non-fouling conditions), increases clearly with pH until appearing over the pressure range studied for pH 6. In Figure 3-d the limit fluxes, J*, are shown as a percentage of the initial one, J_0, for the different applied pressures and pH. This clearly shows that the total reduction in flux is almost constant until a relatively high pressure (increasing with pH) when the flux reduction increases steeply at the pressure for the critical ("weak concept") flux. Of course J* is always below J_0 thus giving always a decrease in flux with time. An initial flux below the "weak concept" critical flux, J_{2c}, would assure a constant resistance in the same way that a flux below the "strong concept" critical flux, J_{1c}, would give the non- fouling (pure water) resistance according to Figure 1.

Figure 3.- The initial and limit fluxes as a function of pressure for (a) pH=4; (b) pH=5 and (c) pH=6. In (d) the limit fluxes are shown in terms of the initial one.

In Figure 4-a, Z/A (charge number per unit of membrane area) is shown as a function of pH. The charge of BSA as a function of pH can be obtained from the literature [***39, 40***]. Vilker et al. [***40***] obtained the corresponding Z values for BSA as shown in Figure 5-a for some pH values.

The protein-to-protein and protein-to-membrane interactions can be assumed as determined substantially by their electrostatic forces and the short range ones around the zero charge state; then they should be proportional to the product of the respective charges (charge and charge density, for the protein and the membrane, respectively) when outside the isoelectric point. These (electrostatical) interactions are also shown in Figures 4-b and 5-b. It is worth noting that the short range forces appearing at the isoelectric point of the protein are responsible for the formation of aggregates and do not appear in the x-axis of Figures 4 to 6 and 8.

Figure 4.- (a) The charge density Z/A for the SB membrane and (b) The electrostatic interaction between BSA and the SB membrane per unit of membrane area.

Figure 5.- The charge Z (a) and electrostatic interaction (b) values for BSA.

In Figure 6, the limit flux J* is shown as a function of the protein-protein electrostatic interaction (Figure 6-a) and of the protein-membrane electrostatic interaction (Figure 6-b). Figure 6-a shows that fouling, in terms of J*, is especially high (low J*) for medium electrostatic protein-protein repulsion (pH = 6).

As mentioned, BSA near the isoelectric point, due to the lack of electrostatic repulsion and the subsequent prevalence of short range attractive forces, form amorphous aggregates by non-specific interactions principally of a hydrophobic nature. These aggregates are likely to be reversible although the magnitude of the relevant equilibrium constants is unknown [***41***]. At pH values far from the BSA isoelectric point, repulsion between molecules reduces aggregation leading to a structural reorganization of the protein and to the formation of β-aggregates involving secondary structure. This results in the growth of simple smaller fibrillar structures, [***42-44***]. When the electrostatic protein-protein interaction (repulsion) is small (pH = 5) or high (pH =6 and 4), the presence of some protein aggregates has low influence on the total flux decay. It is worth noting that no measurement has been done at the exact isoelectric point thus the peak action of these aggregates hasn't been shown.

The question is entirely different when Figure 6-b is examined. There, the protein-membrane electrostatic interaction has a much relevant role in flux decay because it seems clear that increasing membrane-protein repulsion decreases adsorption. Of course this was foreseeable. At pH = 5 big aggregates would also adhere on the membrane due to the amphoteric character of the aggregates while at pH = 4 small aggregates wouldn't be attached on the membrane due to the protein-membrane repulsion. At pH = 6, membrane and protein are attracted by each other and flux is substantially reduced. The size of the aggregates would not play a central role, in this case, because the pores are extremely big, 0.45 mm as compared to the typical size of BSA that un-aggregated is an ellipsoidal protein with the major axis being 14 nm and the minor axis 4 nm [***45***]. When the pores are so wide and for low temperatures and not too low ionic strengths (see Table III) there is no occasion for the BSA molecules to approach each other significantly as to increase by aggregation their size over 450 nm in diameter. At neutral pH BSA has 8 nm effective diameter as measured by Light Scattering [***46***] and initial transmission, through an ultrafiltration membrane of a molecular weight cut-off of 300KDa (equivalent to around 20 nm in pore size), is practically 100% irrespective of pH (from 3 to 7) [***47***]. For filtration times as long as 10000 s the transmission of BSA decreases nearly until 50 %, but then transmission is also quite similar for all the pH range from 3 to 7. This would explain why a relatively mild fouling has been found ~~by us~~ near the isoelectric point, although.

In all cases the effect on J* of the applied pressure (analyzed in Figure 3-d) is clearly of minor relevance, as compared with the effect of the membrane-protein electrostatic interaction when dealing with low pressures. The relevance of particle-particle and particle membrane has been analyzed for example in the works of Bowen et al [***14***], Kim and Zidney, [***48***], and Huysman and coworkers, [***47, 49, 50***]. Bowen et al., [***14***], concluded that a maximization of the zeta potential (charge) of the membrane or pore entrance materials or tuning pH to maximize repulsive membrane-solute interaction would be two convenient strategies to optimize the membrane functionality both increasing retention and improving resistance to fouling. We have shown that these statements

can be subscribed when dealing with the low pressure microfiltration of protein broths because in this case also an electrostatic reduction of pore blocking appears.

Figure 6.- The limit flux as a function of electrostatic interaction: (a) protein-protein and (b) membrane-protein.

In Figure 7, an example of the corresponding fitting of the integral filtration coefficient, Λ, given by Equation (25), to Equation (27) showing clearly that a better fit is obtained for the complete model. The goodness of these fittings can be measured by their coefficient of determination, which has been clearly better always for the complete blocking model. Nevertheless, it is worth mentioning that an only slightly poorer fitting appears for the "standard" or internal pore fouling. These features are general for all pressures and pH.

Figure 7.- The Λ coefficient for: (a) the complete fouling model; (b) the standard model; (c) the intermediate model and (d) the cake model. Data correspond to pH=6 and $\triangle$p= 4.85 KPa.

We have seen that the fouling kinetics, in our case, fits the predictions of complete blocking mechanism by using Equation (11). But actually to get this knowledge we had to make tests for all the possible models each with its β according to Table I and to use the experimental limit flux. An alternative way by using Equation (16) can be used once the complete blocking mechanism was confirmed that allows the simultaneous fitting of J* and α'. As was shown in Figure 2, for example, the experimental and fitted J* values coincide within the error range and, actually, α' coincides also when calculated from Equation (11) or (16). It is worth mentioning here that Equation (9) is inconvenient for a fitting procedure, although it was extraordinarily useful when no limit fluxes appeared, [***30***].

In Figure 8 the dependence of the kinetic constant, K_A/Θ (evaluated as α'/J_0) on pressure and pH is shown. It seems clear that there is a faster decrease in flux in the vicinity of the isoelectric point with a slightly slower decay in flux when there are both membrane-to-protein (see Figure 4-b) and protein-protein repulsion (pH = 4). The slowest kinetics appears for membrane-to-protein attraction (see again Figure 4-b) with protein-protein repulsion (pH = 6). Note that at pH = 6 the kinetics is very slow although fouling is strong giving lower limit fluxes for all the applied pressures (see Figures 3-c and 3-d and Figure 6) with J^*/J_0 around 50%. For pH = 4 there is an especially fast kinetic for intermediate pressures arriving to levels which are characteristic of the protein at the isoelectric point. This should be probably due to the interaction of the small aggregates appearing for pH = 4 to form bigger aggregates, similar to those that appear for pH = 5, higher pressures should saturate this phenomenon.

Figure 8.- The K_A/Θ kinetic constant as a function of: (a) the protein-membrane interaction and (b) the applied pressure, for the pH studied.

5. Conclusions.

The concepts of limit and critical fluxes have been revised and both the concepts have been clearly distinguished and some misunderstandings clarified. The models for the different mechanisms that are

customarily assumed to act in fouling or flux decay phenomena have been included in a common frame encompassing the cases with both zero and non-zero limit fluxes. Within this frame, the standard model that assumes an internal pore deposition has been included as well, for the first time. For cross flow microfiltration this mechanism has been usually ignored but certainly it should be taken into account when the solute or its aggregates are small as compared with pore size as far as the flux, when passing along the pores, could introduce a sweeping or erosive action on the internal deposit. This could be especially relevant when this is the only shear stress source as should be the case for dead end microfiltration. Although as mentioned shear stress is not the only possible factor leading to saturation of deposition or adsorption when dealing with low pressures. In this case, the same shear caused inside the pores on their pore walls should act on the pore entrances explaining the appearance of equilibrium between deposition and removal under other flux decay regimes.

In our case we have seen that when BSA is dead-end microfiltered at low pressures through a positively charged membrane, limit fluxes appear to follow mainly a complete fouling mechanism. In this case the membrane-protein interaction has a relevant action as far as it seems to control both the intensity and kinetics of flux decay. Of course the control of the flux decay is somehow modulated by the protein-protein interaction especially affecting the kinetics in the vicinity of the isoelectric point of the protein when bigger aggregates would appear due to the short range forces. There is a faster flux-decay for PH values near the protein isoelectric point with a slightly slower decline in flux when there are both membrane-to-protein and protein-protein repulsion. The slowest kinetics appears for membrane-to-protein attraction with protein-protein repulsion. Fouling is stronger, and the limit flux smaller, when the protein is attracted towards the membrane and the protein molecules are moderately repelled to each other.

Acknowledgements.

Authors thank the Ministerio de Educación y Ciencia (Plan Nacional de I+D+i) through projects MAT2011-25513 and CTQ2012-31076, Junta de Castilla y León (project VA-324A11-2) and also Acciona Agua for partial funding of this research. We are indebted also to Ministerio de Economía y Productividad through project MAT2010-20668

6. References.

1. Separation processes in the food and biotechnology industries, Principles and Applications, A. S. Grandison and M. J. Lewis, Woodhead Pub. Lmtd, Cambridge, UK, 1996.
2. Y. El Rayess, C. Albasi, P. Bacchin, P. Taillandier, J. Raynal, M. Mietton-Peuchot, A. Devatine, Cross-flow microfiltration applied to oenology: A review, J. Membr. Sci. 382 (2011) 1– 19. doi:10.1016/j.memsci.2011.08.008
3. M. T. Aspelund, Membrane-based separations for solid/liquid clarification and protein purification, PhD Thesis, Univ. Iowa, 2010.
4. C. Charcosset, Membrane Processes in Biotechnologies and Pharmaceutics, Elsevier B.V, Amsterdam, The Netherlands, 2012.

5. A.D. Marshall, P.A. Munro, C. Trägårdh, The effect of protein fouling in microfiltration and ultrafiltration on permeate flux, protein retention and selectivity: a literature review, Desalination 91 (1993) 65-108. doi:10.1016/0011-9164(93)80047-Q
6. W.S. Opong, A.L. Zidney, Hydraulic permeability of protein layers deposited during microfiltration, J. Colloid Interface Sci. 142 (1991) 41-60. doi: 10.1002/bit.260460105
7. S.T. Kelly, W.S. Opong, A.L. Zidney, The influence of protein aggregates on the fouling of microfiltration membranes during stirred cell filtration, J. Membr. Sci. 80 (1993) 175-187. doi:10.1016/0376-7388(93)85142-J
8. W.R. Bowen, Q. Gan, Properties of microfiltration membranes: flux loss during constant pressure permeation of bovine serum albumin, Biotech. Bioeng. 38 (1991) 688-696. doi: 10.1002/bit.260380703
9. E.J. de la Casa, A. Guadix, R. Ibáñez, E.M. Guadix, Influence of pH and salt concentration on the cross-flow microfiltration of BSA through a ceramic membrane, Biochem. Eng. J. 33 (2007) 110–115. doi:10.1016/j.bej.2006.09.009
10. W.R. Bowen and Q. Gan, Properties of microfiltration membranes: the effect of adsorption and shear on the recovery of an enzyme, Biotech. Bioeng. 40 (1992)491-497. doi: 10.1002/bit.260400407
11. W.R. Bowen and Q. Gan, Microfiltration of protein solutions at thin film composite membranes, J. Membr. Sci. 80 (1993) 165-173. doi:10.1016/0376-7388(93)85141-I
12. A.C.M. Franken, J.T.M. Sluys, V. Chen, A.G. Fane, C.J.D. Fell, Role of protein conformation on membrane characteristics, pp. 207-213. In: Proceedings of the Fifth World Filtration Congress, Nice, Vol. 1, Societé Française de Filtration, Cachan, France, 1990.
13. A. Grenier, M. Meireles, P. Aimar, P. Carvin, Analysing flux decline in dead-end filtration, Chem. Eng. Res. Des. 86 (2008) 1281-1293. doi:10.1016/j.cherd.2008.06.005
14. W.R. Bowen, N. Hilal, M. Jain, R.W. Lovitt, A.O. Sharif and C.J. Wright, The effects of electrostatic interactions on the rejection of colloids by membrane pores - visualisation and quantification, Chem. Eng. Eng. Sci. 54(3) (1999) 369-375. doi:10.1016/S0009-2509(98)00252-8
15. P. Bacchin, A possible link between critical and limiting flux for colloidal systems: consideration of critical deposit formation along a membrane, J. Membr. Sci. 228 (2004) 237–241. doi:10.1016/j.memsci.2003.10.012
16. P. Bacchin, P. Aimar and R.W. Field, Critical and sustainable fluxes: theory, experiments and applications, J. Membr. Sci. 281, 1-2 (2006) 42-69. doi:10.1016/j.memsci.2006.04.014
17. P. Bacchin, D. Si-Hassen, V. Starov, M.J Clifton and P Aimar, A unifying model for concentration polarization, gel-layer formation and particle deposition in cross-flow membrane filtration of colloidal suspensions, Chem. Eng. Sci., 57(1) (2002) 77-91. doi:10.1016/S0009-2509(01)00316-5
18. P. Bacchin and P. Aimar, Critical fouling conditions induced by colloidal surface interactions: from causes to consequences, Desalination 175 (2005) 21-27. doi:OI10.1016/j.memsci.2009.06.046

19. B. Espinasse, P. Bacchin, P. Aimar, Filtration method characterizing the reversibility of colloidal fouling layers at a membrane surface: Analysis through flux and osmotic pressure, J. Membr. Sci. 320 (2008) 483-490. doi: 10.1016/j.memsci.2009.06.046
20. R.W. Field, D. Wu, J.A. Howell, B.B. Gupta, Critical flux concept for microfiltration fouling, J. Membr. Sci. 100 (1995) 259-272. doi:10.1016/0376-7388(94)00265-Z
21. G. C. Agbangla, É. Climent, P. Bacchin, Experimental investigation of pore clogging by microparticles: Evidence for a critical flux density of particle yielding arches and deposits, Sep. Purif. Technol. 101 (2012) 42–48. doi:10.1016/j.seppur.2012.09.011
22. R.G.M. van der Sman, H.M. Vollebregt, Transient critical flux due to coupling of fouling mechanisms during crossflow microfiltration of beer, J. Membr. Sci. 435 (2013) 21–37. doi:10.1016/j.memsci.2013.01.015
23. X. Li, J. Li, J. Wang, H. Wang, B. He, H. Zhang, Ultrasonic visualization of sub-critical flux fouling in the double-end submerged hollow fiber membrane module, J. Membr. Sci. 444 (2013) 394–401. doi:10.1016/j.memsci.2013.05.052
24. Y.P. Lim, A. W. Mohammad, Effect of solution chemistry on flux decline during high concentration protein ultrafiltration through a hydrophilic membrane, Chem. Eng. J. 159 (2010) 91–97. doi:10.1016/j.cej.2010.02.044
25. J. Kim, F. A. DiGiano, Critical review. Fouling models for low-pressure membrane systems, Sep. Purif. Technol. 68 (2009) 293–304. doi:10.1016/j.seppur.2009.05.018
26. A.C.M. Franken, Prevention and control of membrane fouling: practical implications and examining recent innovations, DSTI, June 2009.
27. M. Ouammou, N. Tijani, J.I. Calvo, C. Velasco, A. Martín, F. Martínez, F. Tejerina, A. Hernández, Flux decay in protein microfiltration through charged membranes as a function of pH, Colloids Surface A 298 (2007) 267–273. doi: 10.1016/ j.colsurfa.2006.11.006
28. C. Velasco, M. Ouammou, J.I. Calvo, and A. Hernández, Protein fouling in microfiltration: deposition mechanism as a function of pressure for different Ph, J. Colloid Interface Sci. 266 (2003) 148–152. doi:10.1016/S0021-9797(03)00613-1
29. J.I. Calvo, A. Hernández, W.R. Bowen, Flux loss across microporous membranes during permeation of bovine serum albumin, in Membranes Processes and Applications, Proc. X Summer School on Membranes, pp. 261-262, University of Valladolid, Valladolid, Spain, 1993.
30. W.R. Bowen, J.I. Calvo, A. Hernandez, Steps of membrane blocking in flux decline during protein microfiltration, J. Membr. Sci. 101 (1995) 153–165. doi:10.1016/0376-7388(94)00295-A
31. C. Herrero, P. Prádanos, J.I. Calvo, F. Tejerina, A. Hernández, Flux decline in protein microfiltration: influence of operative parameters, J. Colloid Interface Sci. 187 (1997) 344-351. doi: 10.1006/jcis.1996.4662
32. J. Hermia, Constant pressure blocking filtration laws – Application to power-law non-newtonian fluids, Chem. Eng. Res. Des. 60 (1982) 183-187.
33. D. Wu, J.A. Howell, R.W. Field, Critical flux measurement for model colloids, J. Membr. Sci. 152 (1999) 89-98. doi:10.1016/S0376-7388(98)00200-2

34. R. Field, J.J. Wu, Modelling of permeability loss in membrane filtration: Re-examination of fundamental fouling equations and their link to critical flux, Desalination 283 (2011) 68-74. doi:10.1016/j.desal.2011.04.035
35. A. Martín, F. Martínez, L. Palacio, P. Prádanos , A. Hernández, Zeta Potential of Membranes as a function of pH. Optimization of isoelectric point evaluation, J. Membr. Sci., 213 (2003) 225-230. doi:10.1016/S0376-7388(02)00530-6
36. J. O'M. Bockris, A. K. N. Reddy, Comprehensive Modern Electrochemistry. Modern Electrochemistry, Second Edition, in 3 Volumes, Volume 1 IONICS, Plenum Press, New York, 1998.
37. J.I. Calvo, A. Hernández, P. Prádanos, F. Tejerina, Charge Adsorption and Zeta Potential in Cyclopore Membranes, J. Colloid Interface Sci. 181 (1996) 399-412. doi:10.1006/jcis.1996.0397
38. A. Martín, F. Martínez, J. Malfeito, L. Palacio, P. Prádanos and A. Hernández, Zeta Potential of Membranes as a function of pH. Optimization of isoelectric point evaluation, J. Membr. Sci., 213 (2003) 225-230. doi:10.1016/S0376-7388(02)00530-6
39. S. Salgın, U. Salgın, S. Bahadır, Zeta Potentials and Isoelectric Points of Biomolecules: The Effects of Ion Types and Ionic Strengths, Int. J. Electrochem. Sci. 7 (2012) 12404 – 12414.
40. V.L. Vilker, C.K. Colton, K.A. Smith, The Osmotic Pressure of Concentrated Protein Solutions: Effect of Concentration and pH in Saline Solutions of Bovine Serum Albumin, J. Colloid Interface Sci. 79 (1981)548-566. doi:10.1016/0021-9797(81)90106-5
41. M. Lindgren, K. Sorgjerd, P. Hammarstrom, Detection and characterization of aggregates, prefibrillar amyloidogenic oligomers, and protofibrils using fluorescence spectroscopy, Biophys J., 88(6) (2005) 4200-4212. doi:10.1529/biophysj.104.049700
42. L.R . de Young, A.L . Fink, K.A. Dills, Aggregation of Globular Proteins, Acc. Chem. Res. 26 (1993) 614-620. doi: 10.1021/ar00036a002
43. V. Vetri, M. D'Amico, V. Foderà, M. Leone, A. Ponzoni, G. Sberveglieri, V. Militello, Bovine Serum Albumin protofibril-like aggregates formation: Solo but not simple mechanism, Arch. Biochem. Biophys. 508 (2011) 13–24. doi: 10.1016/ j.abb.2011.01.024
44. V. Vetri, F. Librizzi, M. Leone, V. Militello, Thermal aggregation of bovine serum albumin at different pH: Comparison with human serum albumin, Eur. Biophys. J. 36 (2007) 717–725. doi: 10.1007/s00249-007-0196-5
45. T.J. Peters, All about Albumin: Biochemistry, Genetics, and Medical Applications, Academic Press, San Diego, CA, USA, 1996.
46. L. Palacio, C-C. Ho, P. Prádanos, A. Hernández, A.L Zydney., Application of a pore-blockage—Cake-filtration model to protein fouling during microfiltration, J. Membr. Sci., 222 (1-2) (2003) 41-51. doi: 10.1002/bit.10283
47. I. H. Huisman, P. Prádanos, A. Hernández, The effect of protein–protein and protein–membrane interactions on membrane fouling in ultrafiltration, J. Membr. Sci., 4647 (2000) 1–12. doi:10.1016/S0376-7388(00)00501-9

48. M.M. Kim and A.L. Zydney, Particle-particle interactions during normal flow filtration: Model simulations, Chem. Eng. Eng. Sci., 60(15) (2005) 4073-4082. doi: 10.1016 /j.ces.2005.01.029
49. I.H. Huisman and C. Tragardh, Particle transport in crossflow microfiltration - I. Effects of hydrodynamics and diffusion, Chem. Eng. Eng. Sci., 54(2) (1999) 271-280. doi:10.1016/S0009-2509(98)00222-X
50. I.H. Huisman G. Tragardh and C. Tragardh, Particle transport in crossflow microfiltration - II. Effects of particle-particle interactions, Chem. Eng. Eng. Sci., 54(2) (1999) 281-289. doi:10.1016/S0009-2509(98)00223-1

TABLES

Table I.- Values of : α , β, α', γ, $(\gamma\alpha')$ and n for the different blocking mechanisms.

	α	β	α'	γ	$\gamma\alpha'$	n
Complete	$K_A u_0$	2	$J_0 K_A/\Theta$	1	$J_0 K_A/\Theta$	-
Standard	$(2K_B/A_0^{1/2})\, u_0^{1/2}$	3/2	$J_0^{1/2} 2K_B/\Theta$	$\frac{1}{2}\sqrt{J_0}$	$J_0 K_B/\Theta$	2
Intermediate	K_A/A_0	1	K_A/Θ	J_0	$J_0 K_A/\Theta$	1
Cake	$(R_r K_C/A_0^2)\, u_0^{-1}$	0	$J_0^{-1} R_r K_C/\Theta$	$2J_0^2$	$J_0 (2R_r K_C)/\Theta$	1/2

Table II.- Nominal characteristics of the filters used.

Membrane	Mean pore size (μm)	Thickness (μm)	Typical water flow rate[1]	Typical air flow rate[2]	Ion exchange capacity (μeq/disc)
SB-6407	0.45	152.4	12	5	+40

[1] Flow of pure water at 10 psi, in mL/min/cm^2

[2] Flow of air at 10 psi, in L/min/cm^2

Table III.- Ionic Strength and Debye's length for water solution of orthophosphoric (H_3PO_4) acid as a function of pH.

	pH=3	**pH=4**	**pH=5**	**pH=6**
I (mol/L)	0.053	0.0595	0.062	0.075
κ^{-1} **(nm)**	1.3156	1.2460	1.2242	1.1103

	pH=7	pH=8	pH=9	pH=10
I (mol/L)	0.120	0.1455	0.1496	0.150
κ^{-1} (nm)	0.8777	0.7971	0.7862	0.7851

FIGURE CAPTION

Figure 1.- Critical and limit fluxes and steady state flux versus pressure gradients. Actually, the steps in the gradients would be more gradual.

Figure 2.- Flux decay for pH=6 and $\triangle p$= 4.85 KPa. The gray line corresponds to the complete fouling model.

Figure 3.- The initial and limit fluxes for as a function of pressure for (a) pH=4; (b) pH=5 and (c) pH=6. In (d) the limit fluxes are shown in terms of the initial one.

Figure 4.- (a) The charge density Z/A for the SB membrane and (b) The electrostatic interaction between BSA and the SB membrane per unit of membrane area.

Figure 5.- The charge Z (a) and electrostatic interaction (b) values for BSA.

Figure 6.- The limit flux as a function of electrostatic interaction: (a) protein-protein and (b) membrane-protein.

Figure 7.- The Λ coefficient for: (a) the complete fouling model; (b) the standard model; (c) the intermediate model and (d) the cake model. Data correspond to pH=6 and $\triangle p$= 4.85 KPa.

Figure 8.- The K_A/Θ kinetic constant as a function of: (a) the protein-membrane interaction and (b) the applied pressure, for the pH studied.

Flux Kinetics, Limit and Critical Fluxes for Low Pressure Dead-end Microfiltration. The case of BSA Filtration through a Positively Charged Membrane

C. Velasco, J.I. Calvo, Laura Palacio, Javier Carmona, Pedro Prádanos and A. Hernández*

Group of Surfaces and Porous Materials UA UVA-CSIC, Dpto. de Física Aplicada, Paseo de Belén, Facultad de Ciencias Universidad de Valladolid, 47071 Valladolid, Spain.

ABSTRACT

The influence of the applied pressure on the flux decay mechanism during Bovine Serum Albumin (BSA) dead-end microfiltration (MF) has been investigated for a polyethersulfone, positively charged, membrane (SB-6407®) from Pall®. BSA solutions, at pH values of 4, 5 (very close to the protein isoelectric point, IEP) and 6, were micro-filtered through the membrane at different low applied transmembrane pressures.

Although filtration was done in dead-end configuration, limit fluxes appeared for all pressures and pH values studied. The concepts of (long time) limit and critical fluxes and their correlation have been clarified and analysed too. The usual blocking filtration laws have been included in a common frame and both the cases with zero or non-zero limit fluxes have been incorporated. Within this frame, the standard model, that assumes an internal pore deposition, has been included as well; although, in our case, the acting mechanism seems to be mainly the so called complete blocking.

Protein adsorption has been analysed in terms of the protein-protein and protein-membrane electrostatic interactions. There is a faster flux-decay for the protein isoelectric point with a slightly slower decline in flux when there are both membrane-to-protein and protein-protein repulsion. The slowest kinetics appears for membrane-to-protein attraction with protein-protein repulsion. Moreover, adsorption is stronger, and the limit flux smaller, when the protein is attracted towards the membrane and there is protein-protein repulsion.

KEYWORDS

Proteins, Dead-end Microfiltration, Flux decay kinetics, Limit and Critical fluxes, Adsorption.

(*) To whom correspondence should be addressed.
Group of Surfaces and Porous Materials UA UVA-CSIC, Dpto. de Física Aplicada, Paseo de Belén s/n,
Facultad de Ciencias, Universidad de Valladolid, 47071 Valladolid, Spain.
Phone: +34-983423134. Fax: +34-983423013. E-mail: tonhg@termo.uva.es

1. Introduction.

Membrane microfiltration is a well-established procedure in biotechnological and biochemical industries, **[*1-4*]**. Microfiltration membranes are especially adequate for the separation of fine particles with sizes in the range from 0.1 to 10.0 microns, especially in cell recovery from fermentation broths, polishing and sterilization of product solutions. It is also used to separate cell fragments caused by cell disruption for the recovery of intracellular enzymes.

Protein transmission and the rate of filtration during microfiltration of protein solutions has been extensively studied and reviewed, **[5-*9*]**. In fact, the transmission of proteins through microfiltration membranes is usually high. Even so, the rate of filtration of apparently pure protein solutions decreases with time at a constant applied pressure. In some cases, this has been explained in terms of deposition of protein in the front face of the membrane, **[*6*]**. It has also been shown that in such cases the adsorption of protein (BSA) is associated with the deposition of trace quantities of aggregated and/or denaturated protein that act as initiators for the continued deposition of bulk protein, **[*6,7*]**. However, a continuous decrease in filtration rate has also been reported in cases where there is neither deposition nor concentration polarization on the front face of the membrane, **[8,*10-12*]**.

Usually less attention than would be required has been devoted to the applied pressure used to measure the flux decrease linked to pore narrowing or clogging due to adsorption or deposition. A notable exception is the work of Grenier et al., [13], where an extensive analysis of the pressure dependence of deposition parameters is performed in dead-end microfiltration of bentonite suspensions that don't show a non-zero limit flux. In any case, the convenience of a reduction of the operating pressure to decrease pore blocking was already recommended by Bowen et al., [***14***].

The origin of limit fluxes – those reached in stationary conditions after long enough times—is not well understood. It is worth noting that in some texts, the more or less pressure independent fluxes reached after applying high enough pressures have been also called limit fluxes, [***15***]. Here, we will only use "limit fluxes" to refer to the long time stationary flux reached at each constant pressure. The cause of critical fluxes, those appearing for relatively high pressures with a decrease in permeability, is neither well identified nor understood. It is clear, that when there is a high pressure flux plateau with a very low permeability, this critical flux can be attributed to an extreme blockage of pores. We will further discuss the conceptual differences and the correlation of limit and critical fluxes below. Nevertheless, we will not refer here to other conceptually different critical fluxes as, for example, those corresponding to the maximum flux before arriving to an irreversible fouling, [***16-19***].

Limit fluxes were originally attributed to factors like cake erosion or deposit removal or back flux, [***20***]. Actually the introduction or quantification of these limit fluxes has been, from the very beginning, substantially phenomenological, [***21-23***]. Though the limit fluxes were originally introduced for cross-flow microfiltration, they can also appear in dead end microfiltration, [***24, 25***]. Although, of course, the sweeping action of tangential

flow would cause the partial loss of the deposit, other causes, as for example the equilibrium between pressure and the attraction or repulsion between the membrane and the solute or the solute-solute interaction, can play a similar role, by limiting the extension and compactness of the deposit. It seems clear that these subtle balances would be more plausible for low pressures because high pressures would always overcome any other interaction. An extensive review of the different theoretical and experimental methodologies applied to cross-flow and dead-end limit and critical fluxes was presented by Bacchin, Aimar and Field, [16].

In any case, as pointed out by Franken, [***26***], present day micro- and ultrafiltration (as well) equipment is designed and operated with a strong accent on avoiding the rise of membrane resistance. Nearly all membrane installations in water treatment are using a very low transmembrane pressure. Whatever way the phenomenon is described (critical flux, limit flux, low pressure), it all comes down to keep the overall resistance as low as possible. In practice this, however, can lead to very low fluxes and/or to the requirement of huge membrane surfaces, this is why the question on what pressures can be applied to avoid an inconvenient increase of the membrane resistances while keeping the needed membrane within reasonable limits is relevant.

Our aim here is to study how the applied pressure intensity can affect both the intensity and kinetics of flux decay or fouling due to deposition. This for a charged membrane should depend on the solution pH and on the details of the membrane charge. The influence of pH in dead end microfiltration of proteins has been previously addressed by us using BSA and Lysozyme and positive, SB-6407®, and negative membranes, ICE-450®, [***27***], for a relatively high pressure. The influence of pressure for BSA microfiltration was also analyzed, [***28***], with the negatively charged membrane, ICE-450®. In all these cases, the fouling kinetics was clearly faster for high pressures although limit fluxes were always very small and could be considered zero without affecting substantially retention that remained insignificant. Here we will use the positive SB-6407® membrane to microfilter BSA at low pressures and different pH values. We will find non-zero limit fluxes for all pressures and pH and we will analyze the intensity and kinetics of flux decay in terms of both membrane-solute and solute-solute electrostatic interactions.

2. Theory.

2.1. Flux Decay Mechanisms

Usually, the kinetics of flux decline is analysed in terms of different blocking laws which are customarily four, namely: standard blocking, intermediate blocking, cake filtration and complete blocking models, [***29-32***]. In the first of these models, the standard model, it is assumed that the solute molecules or particles are adsorbed onto the walls of the pores decreasing their effective radii. The other three models assume that deposition happens externally. In the complete blocking model each molecule or aggregate (or particle) is assumed to obstruct a pore. In the intermediate model some of the pores clog up while some molecules attach to external non-porous surfaces or on other pre-existent deposits. Finally, in the cake filtration model, a cake can form on the membrane.

For all of these mechanisms, it has been shown, [***29-32***], that there is a common simple characteristic equation:

$$\frac{d^2t}{dV^2} = \alpha\left(\frac{dt}{dV}\right)^{\beta} \quad \textbf{(1)}$$

The physical meanings of the parameters of the four usual models, constants α and β, are well known, **[*29-32*],** and are shown in Table I.

Table I.- Values of : α , β, α', γ, ($\gamma\alpha$') and n for the different blocking mechanisms.

The meaning of the constants involved in α is:

- K_A is the membrane surface blocked per unit of total volume permeated through the membrane
- K_B is the decrease in the cross section area of the pores (due to adsorption on the pore walls) per unit of total permeated volume
- $1/K_C$ is the total permeate volume per unit of membrane area (i.e. per unit of the deposited cake area)
- R_r is the ratio of the hydraulic resistance of the cake to the initial or clean membrane resistance, ($R_r = R_C/R_0$)
- A_0 is the porous surface of the membrane and,
- u_0 is the mean initial velocity of the filtrate.

According to the definition of the permeate flux as $J_V = dV/dt$, Equation (1) can be written as:

$$-\frac{dJ_V}{dt} = \alpha J_V^{3-\beta} \quad \textbf{(2)}$$

This relationship simplifies the process of fitting of the experimental data to obtain the corresponding blocking parameter, β.

If the flux per unit area, $J = J_V / A_m$, is used, Equation (2) reads:

$$-\frac{dJ}{dt} = \alpha' J^{3-\beta}$$
$$\alpha' = \alpha\left(\frac{A_m^2}{A_m^{\beta}}\right) \quad \textbf{(3)}$$

The values of α' are shown in Table I. Note that:

$$J(t=0)=J_0=\frac{J_{V0}}{A_m}$$
$$u_0 = \frac{J_{V0}}{A_0} \quad \textbf{(4)}$$
$$\Theta = \frac{A_0}{A_m}$$

A_0 is the porous transversal area of the membrane and Θ is the surface porosity.

2.2. *Limit Flux*

We can define the limit flux for a given pressure, as the stable flux that is achieved once flux decline ceases for a constant pressure experiment As mentioned, in some cases a limit flux, for long times, appears:

$$J^* = \lim_{t\to\infty} J = \lim_{t\to\infty}\left(\frac{J_V}{A_m}\right) \quad \textbf{(5)}$$

This is common, for example, in cross flow filtration.

Field et al., [***20, 33, 34***], performed some modifications in the models of Hermia, in order to include the possible existence of a J*, for: complete, intermediate and cake mechanisms. The limit flux appeared there linked to the partial removal of the substances deposited on the membrane caused by the tangential flow. As a consequence they transformed Equation (3) to:

$$-\frac{dJ}{dt}J^{\beta-2} = \alpha'\left(J - J^*\right) \quad \textbf{(6)}$$

The constant in the right hand term must be equal to α' in order to recover Equation (3) when J*=0. Of course this is equivalent to:

$$-\frac{dJ_V}{dt}J_V^{\beta-2} = \alpha\left(J_V - J^*_V\right) \quad \textbf{(7)}$$

with $J^*_V = J^*A_m$. This equation can be written in terms of derivatives of time as:

$$\frac{d^2t}{dV^2} - \alpha\left(\frac{dt}{dV}\right)^{\beta} + \alpha J^*_V\left(\frac{dt}{dV}\right)^{\beta+1} = 0 \quad \textbf{(8)}$$

or

$$\frac{d^2t}{dV^2} = \alpha\left[1 - \frac{J^*_V}{J_V}\right]\left(\frac{dt}{dV}\right)^{\beta} \quad \textbf{(9)}$$

Of course, Equation (1) is recovered from Equations (8) or (9) when $J^*_V=0$.

Equation (6) can be rearranged to:

$$\frac{dJ}{dt} = -\alpha'\left(J - J^*\right)J^{2-\beta} \quad \textbf{(10)}$$

or

$$\int \frac{J^{\beta-2}}{J - J^*}dJ = A - \alpha' t \quad \textbf{(11)}$$

with A being a constant of integration. Equation (10) should be adequately integrated.

It can be integrated for the cake fouling i.e. for β =0 [β-2 = -2] to:

$$\frac{J\ln\left(J - J^*\right) - J\ln J + J^*}{JJ^{*2}} = A - \alpha' t \quad \textbf{(12)}$$

The integration for the intermediate fouling i.e. for β =1 [β-2 = -1] leads to:

$$J = \frac{J^* e^{\alpha' J^* t}}{e^{\alpha' J^* t} + J^* A} \quad \textbf{(13)}$$

For standard fouling with β =3/2 [β -2=-1/2]:

$$\left(\frac{1}{\sqrt{J^*}}\right)\ln\left(\frac{\sqrt{J}-\sqrt{J^*}}{\sqrt{J}+\sqrt{J^*}}\right) = A - \alpha' t \quad \textbf{(14)}$$

that could be used by assuming that a limit flux could exist also for the standard fouling, which was not assumed by Field because tangential flow wouldn't lead to any removal of the material deposited inside the pores, although for wide enough pores convection would cause enough shear to act in a similar way. In dead-end filtration especially, convection through the pores could certainly be crucial to reach equilibrium between deposition and removal due to the shear stress introduced along the pore. Other factors can also imply a limit on the increase of adsorption or deposition.

Finally, for the complete blocking for β=2 (β-2=0):

$$J = Ae^{-\alpha' t} + J^* \quad \textbf{(15)}$$

Equation (15), by recalling that $J(t=0)=J_0=J_{V0}/A_m$, gives:

$$\frac{J}{J_0} = \left(1 - \frac{J^*}{J_0}\right)e^{-\alpha' t} + \frac{J^*}{J_0} \quad \textbf{(16)}$$

because $A = J_0 - J^*$ for the complete blocking mechanism. Equivalently, Equations (12), (13) and (14) can be written in terms of J_0 as shown in the next section. It is worth mentioning that Field and Wu [34] re-evaluated the flux versus time relationship for the complete blocking mechanism and concluded that shear stress couldn't explain a non-zero limit flux when removal terms for cross flow could be considered both linearly dependent upon shear stress or proportional to shear stress and inversely proportional to flux, in addition to be proportional to the blocked area. Even in these cases, Equation (16) can be written in the same form, although Field and Wu preferred to avoid naming the long time flux as J* because this limit flux could'nt be due to the shear appearing in cross flow filtration.

2.3. Time Dependence of Flux

It is worth noting that Equations (12-14), lead to 0/0 indeterminations for J*=0. While Equation (15) leads to:

$$J = J_0 e^{-\alpha' t} \quad \textbf{(17)}$$

that could be obtained as well from Equation (3). For the intermediate mechanism:

$$A = \frac{1}{J_0} - \frac{1}{J^*} \quad \textbf{(18)}$$

and applying L'Hopital, the equation for the J versus time dependence for J*=0 is:

$$\frac{J}{J_0} = \frac{1}{\left(1 + J_0 \alpha' t\right)} \quad \textbf{(19)}$$

according to the corresponding result from Equation (3) directly. Similarly, for the standard fouling case:

$$A = \left(\frac{1}{\sqrt{J^*}}\right)\ln\left(\frac{\sqrt{J_0}-\sqrt{J^*}}{\sqrt{J_0}+\sqrt{J^*}}\right) \quad \textbf{(20)}$$

and applying L'Hopital:

$$\frac{J}{J_0} = \frac{1}{\left(1+\frac{\alpha'\sqrt{J_0}}{2}t\right)^2} \quad \textbf{(21)}$$

for J*=0 in accordance again with the corresponding result from Equation (3). Finally for the cake mechanism

$$A = \frac{J\ln\left(J_0 - J^*\right) - J_0 \ln J_0 + J^*}{J_0 J^{*2}} \quad \textbf{(22)}$$

and after application of the L'Hopital rule twice:

$$\frac{J}{J_0} = \frac{1}{\left(1+2\alpha' J_0^2 t\right)^{1/2}} \quad \textbf{(23)}$$

for J*=0, that is once again in agreement with the solution from Equation (3).

Equations (19), (21) and (23) can be written as:

$$\frac{J}{J_0} = \frac{1}{\left(1+\gamma\alpha' t\right)^n} \quad \textbf{(24)}$$

The values of γ , n and $\gamma\alpha$' are shown in Table I.

2.4. General Time Dependence of Flux

In general the integral in Equation (11) will be called here integral filtration coefficient:

$$\Lambda \equiv \int \frac{J^{\beta-2}}{J - J^*} dJ \quad \textbf{(25)}$$

or

$$\Lambda \equiv \int J^{\beta-3} dJ \quad \textbf{(26)}$$

for J*=0.

Therefore, equation (11) would read as:

$$\Lambda = A - \alpha' t$$
$$A = \Lambda_0 \quad \textbf{(27)}$$
$$\alpha' = -\frac{d\Lambda}{dt}$$

This gives a meaning for - Λ as:

$$-\Lambda(t) = \int_{o}^{t} \alpha'(t)\, dt \qquad (28)$$

and of course depends on the meaning for α' for each flux decay mechanism shown in Table I.

It is worth noting that given that the integral filtration coefficient would be linear with t (if α' does not depend on time, as usually assumed for each fouling mechanism) it is easy to test, by using this coefficient, what mechanism is followed. Of course the lack of linearity could be attributed to the presence of a time depending α' as would be the case if a mixture or sequence of several mechanisms were assumed.

2.4. Critical Flux

Field et al. in the seminal paper of 1995 introduced the concept of "critical flux" in membrane technology, [***20, 33***]. It defines a critical value of the permeate flux below which no flux decay would occur. The critical flux should depend on: hydrodynamic forces, transmembrane pressure, electrostatic interaction between feed components and with the membrane surface, etc. Even though it is accepted that low-pressure microfiltration is much more effective than high-pressure microfiltration, the emphasis in the concept of critical flux is that it should be appropriate to start filtration operations at a low flux and increase it until reaching the critical value and this could be done without any, or with a controlled low, decline of flux with time [***20***]. In this way a window of operation should be used where "the membrane resistance remains constant as the flux is increased and thus there is a linear relationship between flux and transmembrane pressure" in words of Franken **[*26*]**.

This also resulted in the definition of a "strong form of critical flux" and a "weak form of critical flux". In the first definition a "strong form" of critical flux, it is reached when flux is not anymore identical to the flux of clean water at the same transmembrane pressure but the slope of the line (and the permeability) is lower than that of the initially clean membrane, [***33***]. In the second definition a "weak form" of the critical flux is reached when the linear relationship between transmembrane pressure and flux ceases. It is worth considering that the "strong concept" critical flux happens when fouling is still low but fast while "weak concept" critical flux is associated with high levels of slow fouling.

The concept of critical flux is different from the limit flux appearing in the preceding sections. It seems clear that, according to Equation (6), the flux doesn't decrease when J=J*, but also that when J<J* the flux should increase, although Field [***20, 33***] included the caveat that dJ/dt =0 for $J_0 \leq J^*$. Of course an increase of the flux would be unreasonable. Actually, the dependence of J* on the applied constant pressure (for a given solution-membrane system) should prevent this to happen because if we started with a reduced pressure in order to have low J, the corresponding J* would also be reduced. Thus it should be always $J_0 \geq J^*$ and because, according again with Equation (6), the time evolution of J with time must be monotonous, this should ensure that J>J* (if J_0 >J*) and that J should decrease always or be J=J* constantly (if J_0=J*).

Another question should be: is there a minimum J_0 (with J>J*), below which J*=J_0 always? If this minimum J_0 (or J*) exists it could be called critical flux J_{1c}. This should correspond to the called "strong form" of critical flux if we assume that J_0 versus △p plot corresponds to that for pure water because initial deposition could not have happened yet. If there were a maximum J* that should be reached from any initial flux J_0 this critical flux should correspond to a "weak form" of critical flux, J_{2c}. In Figure 1 the critical fluxes (strong and weak concepts) are shown schematically in terms of the steady state fluxes J*, and the ΔJ*/Δp gradients, as a function of constant applied pressure. According to Bacchin [***15***], there is a limiting flux corresponding to the flux that can't be surpassed at any pressure, no matter how high it could be, that should be $J_{3c}=3J_{2c}/2$. As mentioned we don't deal with this high pressure limiting flux here.

Figure 1.- Critical and limit fluxes and steady state flux versus pressure gradients. Actually, the steps in the gradients would be more gradual.

2.5. Zeta potentials and Membrane Charge Density

In order to understand the changes in fouling and flux decay kinetics with pH it is useful to think in terms of the membrane-protein and protein-protein interactions that can be interpreted approximately in terms of their (membrane and protein) electrical properties alone. Here we will focus on the electrostatic interaction although it is well known that short range forces play a key role especially near the zero charge conditions (isoelectric point). In this and the next sections, we will pay special attention to the charge of the membrane, while the charge of BSA will be taken from literature (as shown below in Figure 5-a).

It has been shown that, to obtain accurate estimations of zeta potentials, and especially to evaluate the isoelectric point of a membrane, the streaming potential can be measured on or through the membrane [***35***] for an aqueous solution of a salt. When the pores are very narrow, diffusion potentials should appear due to retention and the solution of the Poisson-Boltzmann equation inside the pores can be difficult. Also the shape and tortuosity may be relevant for narrow pores. Nevertheless, for wide-enough pores the treatment of the streaming potential through the pores is easy and this procedure should be preferable because it refers to the actual transport path. No significant differences appear within the streaming potential on and through the membrane when any differences between the surface and inner materials could be expected.

In a steady Poiseuille flow through a capillary channel, a relationship between the streaming potential coefficient (ratio of potential difference △E to the applied pressure gradient △p) and the zeta potential ζ, is described by:

$$\nu_p \equiv \frac{\Delta E}{\Delta p} = \frac{\varepsilon \zeta}{\eta\left(\lambda_0 + \frac{\lambda_s}{r_p}\right)} \qquad \textbf{(29)}$$

Equation (29) is the well-known Helmholtz–Smoluchowski equation. In this equation, the specific surface conductivity λ_s is taken into account along with the electrolyte conductivity λ_0. ε is the dielectric constant, η the viscosity of the electrolyte solution, and r_p the capillary radius. Assuming that the dielectric constant of the solution is very large as compared to that of the membrane material, λ_s / r_p can be neglected in the Helmholtz–Smoluchowski equation, then:

$$\zeta = \nu_p \frac{\mu \lambda_0}{\varepsilon} \tag{30}$$

The charge density on the membrane surface can be obtained by, [***36***]:

$$\sigma = \frac{2\varepsilon RT}{F\kappa^{-1}} \sinh \frac{\bar{\zeta}}{2} \tag{31}$$

Here $\bar{\zeta}$ is the dimensionless zeta potential:

$$\bar{\zeta} = \frac{F\zeta}{2RT} \tag{32}$$

R is the gas constant, T the temperature and F the Faraday constant. Finally κ^{-1} is the Debye's length.

Therefore, by this procedure, the surface charge density on the membrane can be obtained from streaming potential measurements, once the zeta potential has been obtained from Equation (30) and the Debye's length is known. The charge number density (per unit of membrane area) is then easily obtained as $Z/A = \sigma / |e|$ where *e* is the elemental charge.

2.6. Ionic Strength and Debye's Length.

As a consequence of the colloidal behavior of the protein molecules at different pH in an aqueous solution, they are surrounded by an electrical double layer with a thickness given by the Debye's length that can be evaluated according to:

$$\kappa^{-1} = \sqrt{\frac{\varepsilon RT}{F^2 \sum_i z_i^2 c_i}} \tag{33}$$

Here, z_i is the charge number of the i-th charged species in the solution and c_i is its concentration. This expression can be simplified by substitution to:

$$\kappa^{-1} = \frac{0.3041}{\sqrt{I}} \tag{34}$$

This gives the Debye's length in nanometers with the ionic strength:

$$I = \frac{1}{2} \sum_i z_i^2 c_i \tag{35}$$

in mol/L.

3. Experimental.

3.1. Membranes and Chemicals.

We used here polymeric microfiltration membranes, obtained from Pall Co®, consisting in flat disks of 47 mm in diameter. Their pore size is 0.45 μm and they have an anion exchange character. The membranes are called SB-6407® by the manufacturer and consist in polyethersulfone unsupported filters that are strongly positively charged by a patented post-treatment process. Other nominal characteristics of these filters are shown in Table II.

Table II.- Nominal characteristics of the filters used.

Bovine serum albumin (BSA) was obtained from Sigma Aldrich (product no. A-6793). 1 g of BSA was dissolved in 1 L of a buffer solution, consisting in a 0.06 mol/L aqueous solution of pure orthophosphoric acid. pH of the resulting solution was adjusted to 4.0, 5.0 and 6.0 (± 0.1) by stepwise addition of drops of a NaOH concentrated solution. Aqueous solutions $1 \cdot 10^{-3}$ mol/L of KCl from Fluka were used for the streaming potential measurements.

All chemicals were of analytical grade and the water used to prepare the solutions was bidistilled and then Milli-Q treated to be almost free of dissolved ions. Solutions were afterwards kept refrigerated for 6 hours before being used. Then pH was readjusted if necessary.

3.2 Filtration Setup.

Dead-end filtration was performed at constant temperature (295 ± 1 K), in a simple device described elsewhere, **[*31, 37*]**, which allows to maintain a constant applied pressure by a liquid column. The permeated flux is measured by a microbalance connected to a PC computer. The applied pressure was kept constant in the range from 1000 to 7000 ± 10 Pa. It is important to point out that because pressure is applied by using a liquid column, pumping denaturation is prevented. In all cases a totally negligible retention was measured.

3.3 Streaming Potential.

The streaming potential experiments were conducted for relatively high concentrations of KCl as mentioned in section 3.1. KCl, among simple salts, has very similar and high mobility for both the anions and cations, **[*38*]**. The through-the-pores streaming potential (ν_p) measurements were performed by us [***27***] with the experimental device described elsewhere, **[*37*].**

In order to evaluate the ionic strength and the corresponding Debye`s length the dissociation equilibria of the buffer 0.06 mol/L solution of orthophosphoric acid, used to control the different pH, have to be taken into account. The three following equilibria appear. Firstly:

$$H_3PO_4 + H_2O \Leftrightarrow H_2PO_4^- + H_3O^+ \quad \textbf{(36)}$$

$$K_1 = \frac{\left[H_2PO_4^- \right]\left[H_3O^+ \right]}{\left[H_3PO_4 \right]} \quad \textbf{(37)}$$

that predominates for pH lower than 7 with k_1=7,5.10^{-3}. For pH between 7 and 12 the main equilibrium is:

$$H_2PO_4^- + H_2O \Leftrightarrow HPO_4^{-2} + H_3O^+ \quad \textbf{(38)}$$

$$K_2 = \frac{\left[HPO_4^{-2} \right]\left[H_3O^+ \right]}{\left[H_2PO_4^- \right]} \quad \textbf{(39)}$$

with K_2 = 2.10^{-7}. Finally over pH 12 the prevailing equilibrium is:

$$HPO_4^{-2} + H_2O \Leftrightarrow PO_4^{-3} + H_3O^+ \quad \textbf{(40)}$$

$$K_3 = \frac{\left[PO_4^{-3} \right]\left[H_3O^+ \right]}{\left[HPO_4^{-2} \right]} \quad \textbf{(41)}$$

with a constant K_3 = 10^{-12}.

The corresponding values for I, obtained from Equations (37), (39) and (41), and κ^{-1} are shown in Table III.

Table III.- Ionic Strength and Debye's length for water solution of orthophosphoric (H_3PO_4) acid as a function of pH.

4. Results and Discussion.

Figure 2 shows an example of the flux decay (for pH=6 and $\triangle$p= 4.85 KPa) showing how a clear limit flux is reached – in this case after 2 hours of filtration. As already mentioned, although frequently limit fluxes aren't

found for dead end filtration, nothing fundamental forbids the appearance of this phenomenon in any filtration mode provided that there is a mechanism that can avoid indefinite fouling [16].

Figure 2.- Flux decay for pH=6 and Δp= 4.85 KPa. The gray line corresponds to the complete fouling model.

The corresponding limit fluxes are shown in Figure 3, along with the initial ones, for the different pH values studied here. It seems clear that fouling increases for increasing pH, in terms of a clear decrease of J*. Note that the initial flux is very approximately equal for all pH values as should correspond to the pure non fouling permeation. Small differences could be attributed to the ambiguities in a correct identification of the zero-time flux, although at the isoelectric point there is a slightly higher initial flux that could be due to a delay in the time of arrival to the membrane of the large aggregates. The identity of pure pure-water fluxes and the initial fluxes were confirmed, within the error range, by measuring those for all pH and pressures used here.

The critical flux corresponding to the maximal flux with no decrease of resistance – "strong concept" critical flux, which is marked with a square, ⊞, in Figure 3 –, decreases with increasing pH to be essentially zero at pH 6. On the other hand, the "weak concept" critical flux, marked as ⊕ in Figure 3, that corresponds to the maximum flux with constant resistance (but lower than that in non-fouling conditions), increases clearly with pH until appearing over the pressure range studied for pH 6. In Figure 3-d the limit fluxes, J*, are shown as a percentage of the initial one, J_0, for the different applied pressures and pH. This clearly shows that the total reduction in flux is almost constant until a relatively high pressure (increasing with pH) when the flux reduction increases steeply at the pressure for the critical ("weak concept") flux. Of course J* is always below J_0 thus giving always a decrease in flux with time. An initial flux below the "weak concept" critical flux, J_{2c}, would assure a constant resistance in the same way that a flux below the "strong concept" critical flux, J_{1c}, would give the non- fouling (pure water) resistance according to Figure 1.

Figure 3.- The initial and limit fluxes as a function of pressure for (a) pH=4; (b) pH=5 and (c) pH=6. In (d) the limit fluxes are shown in terms of the initial one.

In Figure 4-a, Z/A (charge number per unit of membrane area) is shown as a function of pH. The charge of BSA as a function of pH can be obtained from the literature [***39, 40***]. Vilker et al. [***40***] obtained the corresponding Z values for BSA as shown in Figure 5-a for some pH values.

The protein-to-protein and protein-to-membrane interactions can be assumed as determined substantially by their electrostatic forces and the short range ones around the zero charge state; then they should be proportional to the product of the respective charges (charge and charge density, for the protein and the membrane, respectively) when outside the isoelectric point. These (electrostatical) interactions are also shown in Figures 4-b and 5-b. It is worth noting that the short range forces appearing at the isoelectric point of the protein are responsible for the formation of aggregates and do not appear in the x-axis of Figures 4 to 6 and 8.

Figure 4.- (a) The charge density Z/A for the SB membrane and (b) The electrostatic interaction between BSA and the SB membrane per unit of membrane area.

Figure 5.- The charge Z (a) and electrostatic interaction (b) values for BSA.

In Figure 6, the limit flux J* is shown as a function of the protein-protein electrostatic interaction (Figure 6-a) and of the protein-membrane electrostatic interaction (Figure 6-b). Figure 6-a shows that fouling, in terms of J*, is especially high (low J*) for medium electrostatic protein-protein repulsion (pH = 6).

As mentioned, BSA near the isoelectric point, due to the lack of electrostatic repulsion and the subsequent prevalence of short range attractive forces, form amorphous aggregates by non-specific interactions principally of a hydrophobic nature. These aggregates are likely to be reversible although the magnitude of the relevant equilibrium constants is unknown [***41***]. At pH values far from the BSA isoelectric point, repulsion between molecules reduces aggregation leading to a structural reorganization of the protein and to the formation of β-aggregates involving secondary structure. This results in the growth of simple smaller fibrillar structures, [***42-44***]. When the electrostatic protein-protein interaction (repulsion) is small (pH = 5) or high (pH =6 and 4), the presence of some protein aggregates has low influence on the total flux decay. It is worth noting that no measurement has been done at the exact isoelectric point thus the peak action of these aggregates hasn't been shown.

The question is entirely different when Figure 6-b is examined. There, the protein-membrane electrostatic interaction has a much relevant role in flux decay because it seems clear that increasing membrane-protein repulsion decreases adsorption. Of course this was foreseeable. At pH = 5 big aggregates would also adhere on the membrane due to the amphoteric character of the aggregates while at pH = 4 small aggregates wouldn't be attached on the membrane due to the protein-membrane repulsion. At pH = 6, membrane and protein are attracted by each other and flux is substantially reduced. The size of the aggregates would not play a central role, in this case, because the pores are extremely big, 0.45 mm as compared to the typical size of BSA that un-aggregated is an ellipsoidal protein with the major axis being 14 nm and the minor axis 4 nm [***45***]. When the pores are so wide and for low temperatures and not too low ionic strengths (see Table III) there is no occasion for the BSA molecules to approach each other significantly as to increase by aggregation their size over 450 nm in diameter. At neutral pH BSA has 8 nm effective diameter as measured by Light Scattering [***46***] and initial transmission, through an ultrafiltration membrane of a molecular weight cut-off of 300KDa (equivalent to around 20 nm in pore size), is practically 100% irrespective of pH (from 3 to 7) [***47***]. For filtration times as long as 10000 s the transmission of BSA decreases nearly until 50 %, but then transmission is also quite similar for all the pH range from 3 to 7. This would explain why a relatively mild fouling has been found near the isoelectric point, although.

In all cases the effect on J* of the applied pressure (analyzed in Figure 3-d) is clearly of minor relevance, as compared with the effect of the membrane-protein electrostatic interaction when dealing with low pressures. The relevance of particle-particle and particle membrane has been analyzed for example in the works of Bowen et al [***14***], Kim and Zidney, [***48***], and Huysman and coworkers, [***47, 49, 50***]. Bowen et al., [***14***], concluded that a maximization of the zeta potential (charge) of the membrane or pore entrance materials or tuning pH to maximize repulsive membrane-solute interaction would be two convenient strategies to optimize the membrane functionality both increasing retention and improving resistance to fouling. We have shown that these statements

can be subscribed when dealing with the low pressure microfiltration of protein broths because in this case also an electrostatic reduction of pore blocking appears.

Figure 6.- The limit flux as a function of electrostatic interaction: (a) protein-protein and (b) membrane-protein.

In Figure 7, an example of the corresponding fitting of the integral filtration coefficient, Λ, given by Equation (25), to Equation (27) showing clearly that a better fit is obtained for the complete model. The goodness of these fittings can be measured by their coefficient of determination, which has been clearly better always for the complete blocking model. Nevertheless, it is worth mentioning that an only slightly poorer fitting appears for the "standard" or internal pore fouling. These features are general for all pressures and pH.

Figure 7.- The Λ coefficient for: (a) the complete fouling model; (b) the standard model; (c) the intermediate model and (d) the cake model. Data correspond to pH=6 and $\triangle p$= 4.85 KPa.

We have seen that the fouling kinetics, in our case, fits the predictions of complete blocking mechanism by using Equation (11). But actually to get this knowledge we had to make tests for all the possible models each with its β according to Table I and to use the experimental limit flux. An alternative way by using Equation (16) can be used once the complete blocking mechanism was confirmed that allows the simultaneous fitting of J* and α'. As was shown in Figure 2, for example, the experimental and fitted J* values coincide within the error range and, actually, α' coincides also when calculated from Equation (11) or (16). It is worth mentioning here that Equation (9) is inconvenient for a fitting procedure, although it was extraordinarily useful when no limit fluxes appeared, [***30***].

In Figure 8 the dependence of the kinetic constant, K_A/Θ (evaluated as α'/J_0) on pressure and pH is shown. It seems clear that there is a faster decrease in flux in the vicinity of the isoelectric point with a slightly slower decay in flux when there are both membrane-to-protein (see Figure 4-b) and protein-protein repulsion (pH = 4). The slowest kinetics appears for membrane-to-protein attraction (see again Figure 4-b) with protein-protein repulsion (pH = 6). Note that at pH = 6 the kinetics is very slow although fouling is strong giving lower limit fluxes for all the applied pressures (see Figures 3-c and 3-d and Figure 6) with J^*/J_0 around 50%. For pH = 4 there is an especially fast kinetic for intermediate pressures arriving to levels which are characteristic of the protein at the isoelectric point. This should be probably due to the interaction of the small aggregates appearing for pH = 4 to form bigger aggregates, similar to those that appear for pH = 5, higher pressures should saturate this phenomenon.

Figure 8.- The K_A/Θ kinetic constant as a function of: (a) the protein-membrane interaction and (b) the applied pressure, for the pH studied.

5. Conclusions.

The concepts of limit and critical fluxes have been revised and both the concepts have been clearly distinguished and some misunderstandings clarified. The models for the different mechanisms that are

customarily assumed to act in fouling or flux decay phenomena have been included in a common frame encompassing the cases with both zero and non-zero limit fluxes. Within this frame, the standard model that assumes an internal pore deposition has been included as well, for the first time. For cross flow microfiltration this mechanism has been usually ignored but certainly it should be taken into account when the solute or its aggregates are small as compared with pore size as far as the flux, when passing along the pores, could introduce a sweeping or erosive action on the internal deposit. This could be especially relevant when this is the only shear stress source as should be the case for dead end microfiltration. Although as mentioned shear stress is not the only possible factor leading to saturation of deposition or adsorption when dealing with low pressures. In this case, the same shear caused inside the pores on their pore walls should act on the pore entrances explaining the appearance of equilibrium between deposition and removal under other flux decay regimes.

In our case we have seen that when BSA is dead-end microfiltered at low pressures through a positively charged membrane, limit fluxes appear to follow mainly a complete fouling mechanism. In this case the membrane-protein interaction has a relevant action as far as it seems to control both the intensity and kinetics of flux decay. Of course the control of the flux decay is somehow modulated by the protein-protein interaction especially affecting the kinetics in the vicinity of the isoelectric point of the protein when bigger aggregates would appear due to the short range forces. There is a faster flux-decay for PH values near the protein isoelectric point with a slightly slower decline in flux when there are both membrane-to-protein and protein-protein repulsion. The slowest kinetics appears for membrane-to-protein attraction with protein-protein repulsion. Fouling is stronger, and the limit flux smaller, when the protein is attracted towards the membrane and the protein molecules are moderately repelled to each other.

Acknowledgements.

Authors thank the Ministerio de Educación y Ciencia (Plan Nacional de I+D+i) through projects MAT2011-25513 and CTQ2012-31076, Junta de Castilla y León (project VA-324A11-2) and also Acciona Agua for partial funding of this research. We are indebted also to Ministerio de Economía y Productividad through project MAT2010-20668

6. References.

1. Separation processes in the food and biotechnology industries, Principles and Applications, A. S. Grandison and M. J. Lewis, Woodhead Pub. Lmtd, Cambridge, UK, 1996.
2. Y. El Rayess, C. Albasi, P. Bacchin, P. Taillandier, J. Raynal, M. Mietton-Peuchot, A. Devatine, Cross-flow microfiltration applied to oenology: A review, J. Membr. Sci. 382 (2011) 1– 19. doi:10.1016/j.memsci.2011.08.008
3. M. T. Aspelund, Membrane-based separations for solid/liquid clarification and protein purification, PhD Thesis, Univ. Iowa, 2010.
4. C. Charcosset, Membrane Processes in Biotechnologies and Pharmaceutics, Elsevier B.V, Amsterdam, The Netherlands, 2012.

5. A.D. Marshall, P.A. Munro, C. Trägårdh, The effect of protein fouling in microfiltration and ultrafiltration on permeate flux, protein retention and selectivity: a literature review, Desalination 91 (1993) 65-108. doi:10.1016/0011-9164(93)80047-Q
6. W.S. Opong, A.L. Zidney, Hydraulic permeability of protein layers deposited during microfiltration, J. Colloid Interface Sci. 142 (1991) 41-60. doi: 10.1002/bit.260460105
7. S.T. Kelly, W.S. Opong, A.L. Zidney, The influence of protein aggregates on the fouling of microfiltration membranes during stirred cell filtration, J. Membr. Sci. 80 (1993) 175-187. doi:10.1016/0376-7388(93)85142-J
8. W.R. Bowen, Q. Gan, Properties of microfiltration membranes: flux loss during constant pressure permeation of bovine serum albumin, Biotech. Bioeng. 38 (1991) 688-696. doi: 10.1002/bit.260380703
9. E.J. de la Casa, A. Guadix, R. Ibáñez, E.M. Guadix, Influence of pH and salt concentration on the cross-flow microfiltration of BSA through a ceramic membrane, Biochem. Eng. J. 33 (2007) 110–115. doi:10.1016/j.bej.2006.09.009
10. W.R. Bowen and Q. Gan, Properties of microfiltration membranes: the effect of adsorption and shear on the recovery of an enzyme, Biotech. Bioeng. 40 (1992)491-497. doi: 10.1002/bit.260400407
11. W.R. Bowen and Q. Gan, Microfiltration of protein solutions at thin film composite membranes, J. Membr. Sci. 80 (1993) 165-173. doi:10.1016/0376-7388(93)85141-I
12. A.C.M. Franken, J.T.M. Sluys, V. Chen, A.G. Fane, C.J.D. Fell, Role of protein conformation on membrane characteristics, pp. 207-213. In: Proceedings of the Fifth World Filtration Congress, Nice, Vol. 1, Societé Française de Filtration, Cachan, France, 1990.
13. A. Grenier, M. Meireles, P. Aimar, P. Carvin, Analysing flux decline in dead-end filtration, Chem. Eng. Res. Des. 86 (2008) 1281-1293. doi:10.1016/j.cherd.2008.06.005
14. W.R. Bowen, N. Hilal, M. Jain, R.W. Lovitt, A.O. Sharif and C.J. Wright, The effects of electrostatic interactions on the rejection of colloids by membrane pores - visualisation and quantification, Chem. Eng. Eng. Sci. 54(3) (1999) 369-375. doi:10.1016/S0009-2509(98)00252-8
15. P. Bacchin, A possible link between critical and limiting flux for colloidal systems: consideration of critical deposit formation along a membrane, J. Membr. Sci. 228 (2004) 237–241. doi:10.1016/j.memsci.2003.10.012
16. P. Bacchin, P. Aimar and R.W. Field, Critical and sustainable fluxes: theory, experiments and applications, J. Membr. Sci. 281, 1-2 (2006) 42-69. doi:10.1016/j.memsci.2006.04.014
17. P. Bacchin, D. Si-Hassen, V. Starov, M.J Clifton and P Aimar, A unifying model for concentration polarization, gel-layer formation and particle deposition in cross-flow membrane filtration of colloidal suspensions, Chem. Eng. Sci., 57(1) (2002) 77-91. doi:10.1016/S0009-2509(01)00316-5
18. P. Bacchin and P. Aimar, Critical fouling conditions induced by colloidal surface interactions: from causes to consequences, Desalination 175 (2005) 21-27. doi:OI10.1016/j.memsci.2009.06.046

19. B. Espinasse, P. Bacchin, P. Aimar, Filtration method characterizing the reversibility of colloidal fouling layers at a membrane surface: Analysis through flux and osmotic pressure, J. Membr. Sci. 320 (2008) 483-490. doi: 10.1016/j.memsci.2009.06.046
20. R.W. Field, D. Wu, J.A. Howell, B.B. Gupta, Critical flux concept for microfiltration fouling, J. Membr. Sci. 100 (1995) 259-272. doi:10.1016/0376-7388(94)00265-Z
21. G. C. Agbangla, É. Climent, P. Bacchin, Experimental investigation of pore clogging by microparticles: Evidence for a critical flux density of particle yielding arches and deposits, Sep. Purif. Technol. 101 (2012) 42–48. doi:10.1016/j.seppur.2012.09.011
22. R.G.M. van der Sman, H.M. Vollebregt, Transient critical flux due to coupling of fouling mechanisms during crossflow microfiltration of beer, J. Membr. Sci. 435 (2013) 21–37. doi:10.1016/j.memsci.2013.01.015
23. X. Li, J. Li, J. Wang, H. Wang, B. He, H. Zhang, Ultrasonic visualization of sub-critical flux fouling in the double-end submerged hollow fiber membrane module, J. Membr. Sci. 444 (2013) 394–401. doi:10.1016/j.memsci.2013.05.052
24. Y.P. Lim, A. W. Mohammad, Effect of solution chemistry on flux decline during high concentration protein ultrafiltration through a hydrophilic membrane, Chem. Eng. J. 159 (2010) 91–97. doi:10.1016/j.cej.2010.02.044
25. J. Kim, F. A. DiGiano, Critical review. Fouling models for low-pressure membrane systems, Sep. Purif. Technol. 68 (2009) 293–304. doi:10.1016/j.seppur.2009.05.018
26. A.C.M. Franken, Prevention and control of membrane fouling: practical implications and examining recent innovations, DSTI, June 2009.
27. M. Ouammou, N. Tijani, J.I. Calvo, C. Velasco, A. Martín, F. Martínez, F. Tejerina, A. Hernández, Flux decay in protein microfiltration through charged membranes as a function of pH, Colloids Surface A 298 (2007) 267–273. doi: 10.1016/ j.colsurfa.2006.11.006
28. C. Velasco, M. Ouammou, J.I. Calvo, and A. Hernández, Protein fouling in microfiltration: deposition mechanism as a function of pressure for different Ph, J. Colloid Interface Sci. 266 (2003) 148–152. doi:10.1016/S0021-9797(03)00613-1
29. J.I. Calvo, A. Hernández, W.R. Bowen, Flux loss across microporous membranes during permeation of bovine serum albumin, in Membranes Processes and Applications, Proc. X Summer School on Membranes, pp. 261-262, University of Valladolid, Valladolid, Spain, 1993.
30. W.R. Bowen, J.I. Calvo, A. Hernandez, Steps of membrane blocking in flux decline during protein microfiltration, J. Membr. Sci. 101 (1995) 153–165. doi:10.1016/0376-7388(94)00295-A
31. C. Herrero, P. Prádanos, J.I. Calvo, F. Tejerina, A. Hernández, Flux decline in protein microfiltration: influence of operative parameters, J. Colloid Interface Sci. 187 (1997) 344-351. doi: 10.1006/jcis.1996.4662
32. J. Hermia, Constant pressure blocking filtration laws – Application to power-law non-newtonian fluids, Chem. Eng. Res. Des. 60 (1982) 183-187.
33. D. Wu, J.A. Howell, R.W. Field, Critical flux measurement for model colloids, J. Membr. Sci. 152 (1999) 89-98. doi:10.1016/S0376-7388(98)00200-2

34. R. Field, J.J. Wu, Modelling of permeability loss in membrane filtration: Re-examination of fundamental fouling equations and their link to critical flux, Desalination 283 (2011) 68-74. doi:10.1016/j.desal.2011.04.035
35. A. Martín, F. Martínez, L. Palacio, P. Prádanos , A. Hernández, Zeta Potential of Membranes as a function of pH. Optimization of isoelectric point evaluation, J. Membr. Sci., 213 (2003) 225-230. doi:10.1016/S0376-7388(02)00530-6
36. J. O'M. Bockris, A. K. N. Reddy, Comprehensive Modern Electrochemistry. Modern Electrochemistry, Second Edition, in 3 Volumes, Volume 1 IONICS, Plenum Press, New York, 1998.
37. J.I. Calvo, A. Hernández, P. Prádanos, F. Tejerina, Charge Adsorption and Zeta Potential in Cyclopore Membranes, J. Colloid Interface Sci. 181 (1996) 399-412. doi:10.1006/jcis.1996.0397
38. A. Martín, F. Martínez, J. Malfeito, L. Palacio, P. Prádanos and A. Hernández, Zeta Potential of Membranes as a function of pH. Optimization of isoelectric point evaluation, J. Membr. Sci., 213 (2003) 225-230. doi:10.1016/S0376-7388(02)00530-6
39. S. Salgın, U. Salgın, S. Bahadır, Zeta Potentials and Isoelectric Points of Biomolecules: The Effects of Ion Types and Ionic Strengths, Int. J. Electrochem. Sci. 7 (2012) 12404 – 12414.
40. V.L. Vilker, C.K. Colton, K.A. Smith, The Osmotic Pressure of Concentrated Protein Solutions: Effect of Concentration and pH in Saline Solutions of Bovine Serum Albumin, J. Colloid Interface Sci. 79 (1981)548-566. doi:10.1016/0021-9797(81)90106-5
41. M. Lindgren, K. Sorgjerd, P. Hammarstrom, Detection and characterization of aggregates, prefibrillar amyloidogenic oligomers, and protofibrils using fluorescence spectroscopy, Biophys J., 88(6) (2005) 4200-4212. doi:10.1529/biophysj.104.049700
42. L.R . de Young, A.L . Fink, K.A. Dills, Aggregation of Globular Proteins, Acc. Chem. Res. 26 (1993) 614-620. doi: 10.1021/ar00036a002
43. V. Vetri, M. D'Amico, V. Foderà, M. Leone, A. Ponzoni, G. Sberveglieri, V. Militello, Bovine Serum Albumin protofibril-like aggregates formation: Solo but not simple mechanism, Arch. Biochem. Biophys. 508 (2011) 13–24. doi: 10.1016/ j.abb.2011.01.024
44. V. Vetri, F. Librizzi, M. Leone, V. Militello, Thermal aggregation of bovine serum albumin at different pH: Comparison with human serum albumin, Eur. Biophys. J. 36 (2007) 717–725. doi: 10.1007/s00249-007-0196-5
45. T.J. Peters, All about Albumin: Biochemistry, Genetics, and Medical Applications, Academic Press, San Diego, CA, USA, 1996.
46. L. Palacio, C-C. Ho, P. Prádanos, A. Hernández, A.L Zydney., Application of a pore-blockage—Cake-filtration model to protein fouling during microfiltration, J. Membr. Sci., 222 (1-2) (2003) 41-51. doi: 10.1002/bit.10283
47. I. H. Huisman, P. Prádanos, A. Hernández, The effect of protein–protein and protein–membrane interactions on membrane fouling in ultrafiltration, J. Membr. Sci., 4647 (2000) 1–12. doi:10.1016/S0376-7388(00)00501-9

48. M.M. Kim and A.L. Zydney, Particle-particle interactions during normal flow filtration: Model simulations, Chem. Eng. Eng. Sci., 60(15) (2005) 4073-4082. doi: 10.1016 /j.ces.2005.01.029
49. I.H. Huisman and C. Tragardh, Particle transport in crossflow microfiltration - I. Effects of hydrodynamics and diffusion, Chem. Eng. Eng. Sci., 54(2) (1999) 271-280. doi:10.1016/S0009-2509(98)00222-X
50. I.H. Huisman G. Tragardh and C. Tragardh, Particle transport in crossflow microfiltration - II. Effects of particle-particle interactions, Chem. Eng. Eng. Sci., 54(2) (1999) 281-289. doi:10.1016/S0009-2509(98)00223-1

TABLES

Table I.- Values of : α , β, α', γ, $(\gamma\alpha')$ and n for the different blocking mechanisms.

	α	β	α'	γ	$\gamma\alpha'$	n
Complete	$K_A u_0$	2	$J_0 K_A/\Theta$	1	$J_0 K_A/\Theta$	-
Standard	$(2K_B/A_0^{1/2})\, u_0^{1/2}$	3/2	$J_0^{1/2} 2K_B/\Theta$	$\frac{1}{2}\sqrt{J_0}$	$J_0 K_B/\Theta$	2
Intermediate	K_A/A_0	1	K_A/Θ	J_0	$J_0 K_A/\Theta$	1
Cake	$(R_r K_C/A_0^2)\, u_0^{-1}$	0	$J_0^{-1} R_r K_C/\Theta$	$2J_0^2$	$J_0 (2R_r K_C)/\Theta$	1/2

Table II.- Nominal characteristics of the filters used.

Membrane	Mean pore size (μm)	Thickness (μm)	Typical water flow rate[1]	Typical air flow rate[2]	Ion exchange capacity (μeq/disc)
SB-6407	0.45	152.4	12	5	+40

[1] Flow of pure water at 10 psi, in mL/min/cm^2

[2] Flow of air at 10 psi, in L/min/cm^2

Table III.- Ionic Strength and Debye's length for water solution of orthophosphoric (H_3PO_4) acid as a function of pH.

	pH=3	**pH=4**	**pH=5**	**pH=6**
I (mol/L)	0.053	0.0595	0.062	0.075
κ^{-1} **(nm)**	1.3156	1.2460	1.2242	1.1103

	pH=7	pH=8	pH=9	pH=10
I (mol/L)	0.120	0.1455	0.1496	0.150
κ^{-1} (nm)	0.8777	0.7971	0.7862	0.7851

FIGURE CAPTION

Figure 1.- Critical and limit fluxes and steady state flux versus pressure gradients. Actually, the steps in the gradients would be more gradual.

Figure 2.- Flux decay for pH=6 and $\triangle p$= 4.85 KPa. The gray line corresponds to the complete fouling model.

Figure 3.- The initial and limit fluxes for as a function of pressure for (a) pH=4; (b) pH=5 and (c) pH=6. In (d) the limit fluxes are shown in terms of the initial one.

Figure 4.- (a) The charge density Z/A for the SB membrane and (b) The electrostatic interaction between BSA and the SB membrane per unit of membrane area.

Figure 5.- The charge Z (a) and electrostatic interaction (b) values for BSA.

Figure 6.- The limit flux as a function of electrostatic interaction: (a) protein-protein and (b) membrane-protein.

Figure 7.- The Λ coefficient for: (a) the complete fouling model; (b) the standard model; (c) the intermediate model and (d) the cake model. Data correspond to pH=6 and $\triangle p$= 4.85 KPa.

Figure 8.- The K_A/Θ kinetic constant as a function of: (a) the protein-membrane interaction and (b) the applied pressure, for the pH studied.

Figure
Click here to download Figure: 15-01-15-Figures-Velascoetal.pptx

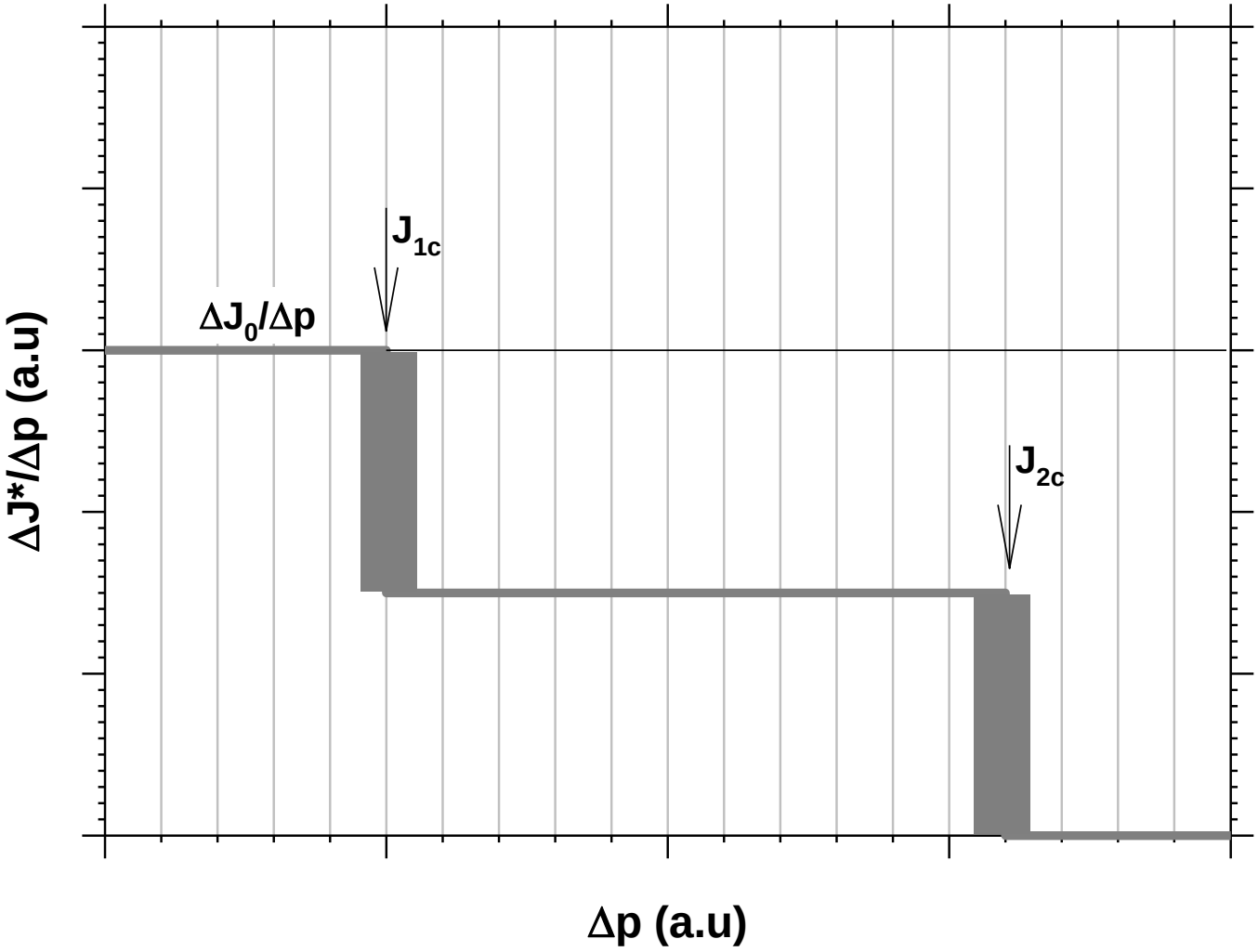

Figure 1.- Critical and limit fluxes and steady state flux versus pressure gradients. Actually, the steps in the gradients would be more gradual.

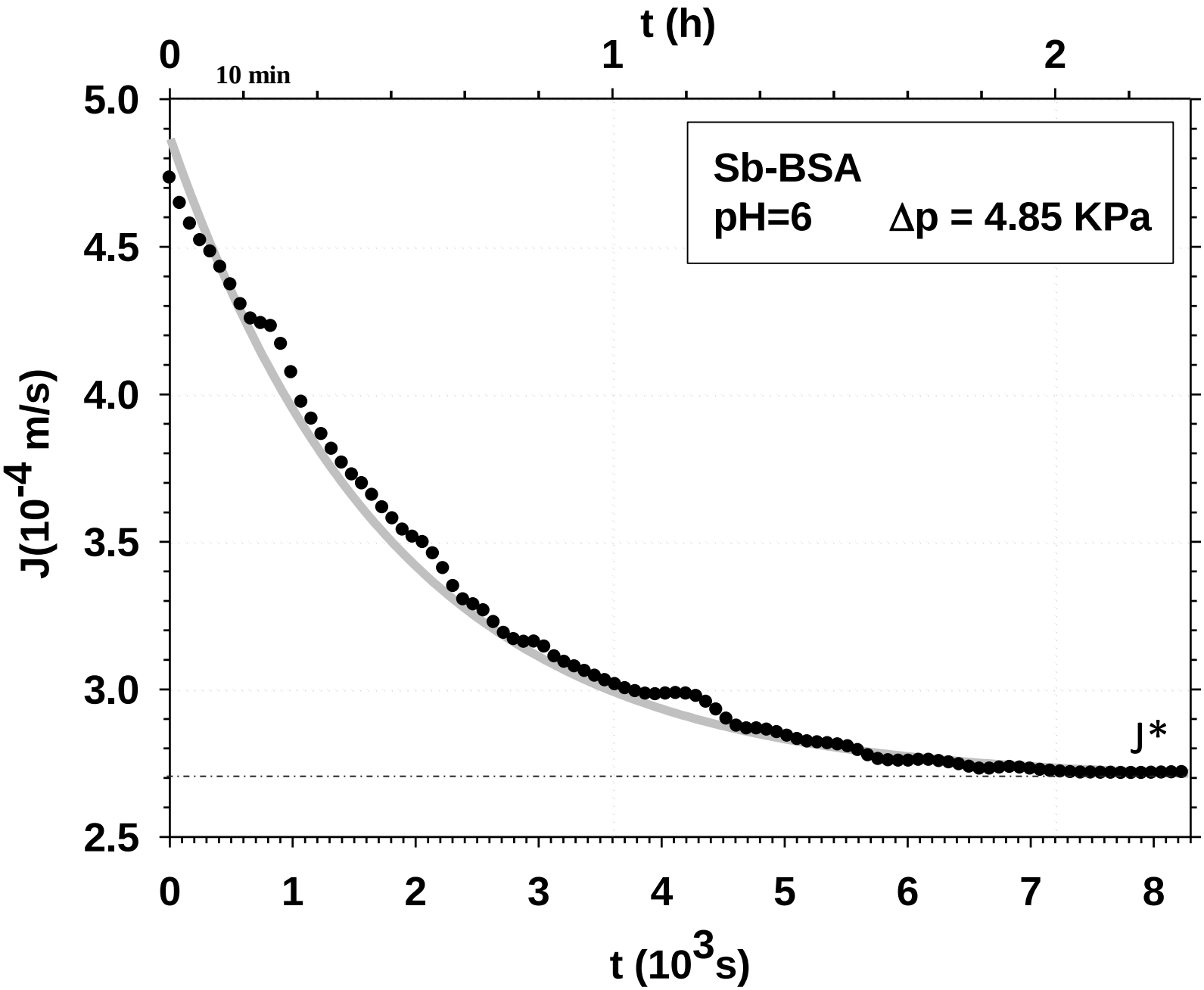

Figure 2.- Flux decay for pH = 6 and △p= 4.85 KPa. The gray line corresponds to the complete fouling model.

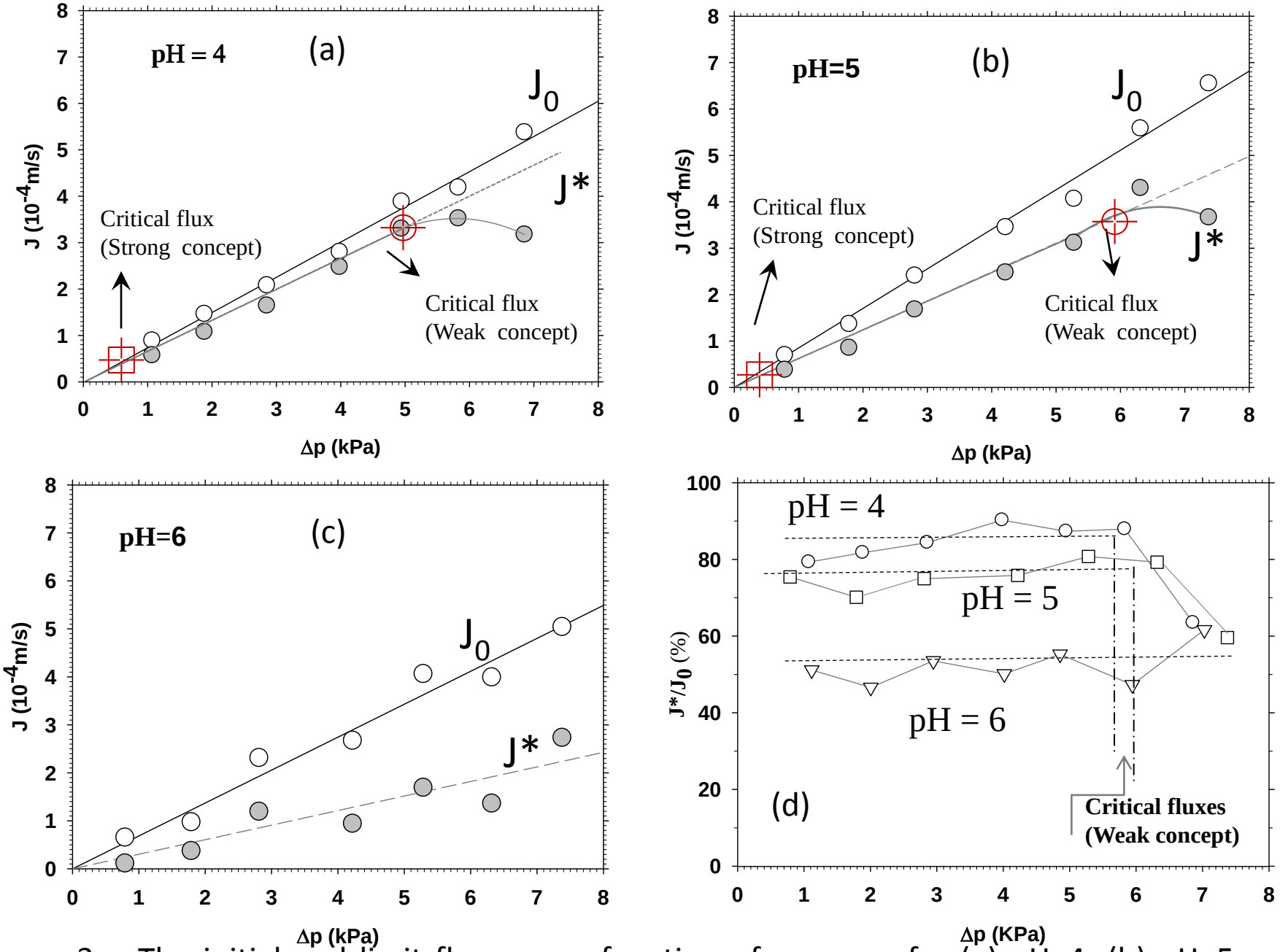

Figure 3.- The initial and limit fluxes as a function of pressure for (a) pH=4; (b) pH=5 and (c) pH=6. In (d) the limit fluxes are shown in terms of the initial one.

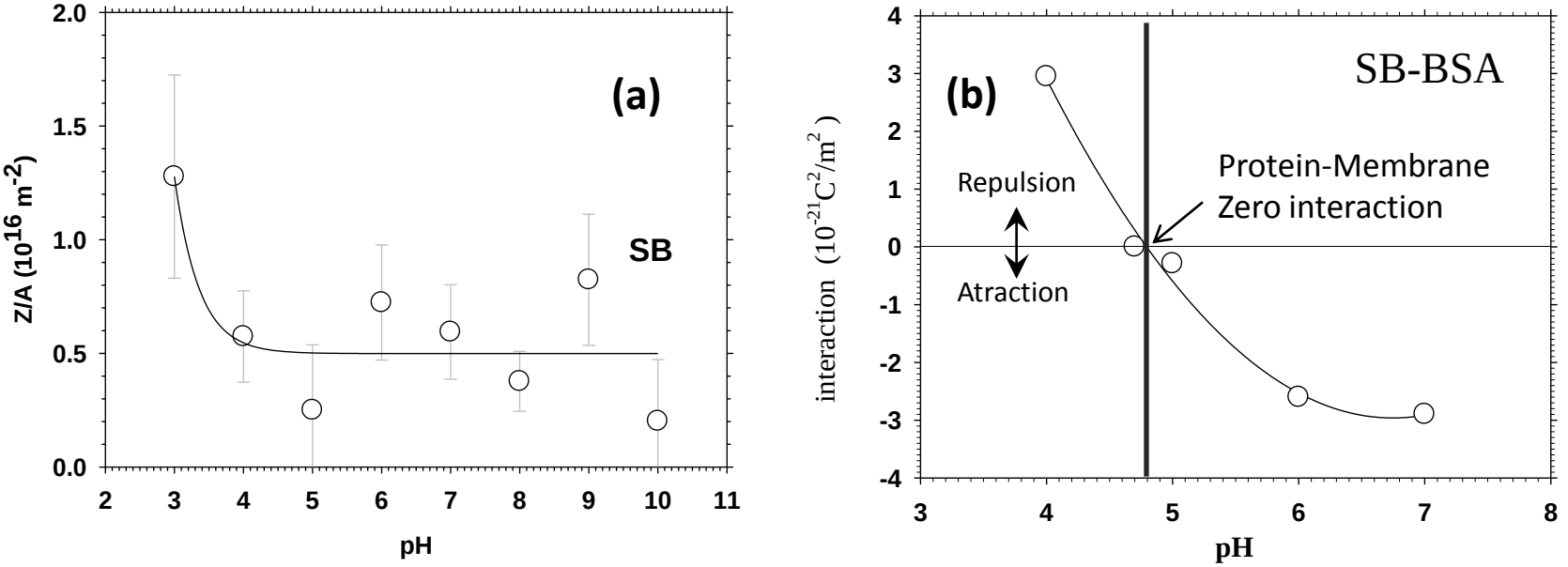

Figure 4.- (a) The charge density Z/A for the SB membrane and (b) The electrostatic interaction between BSA and the SB membrane per unit of membrane area.

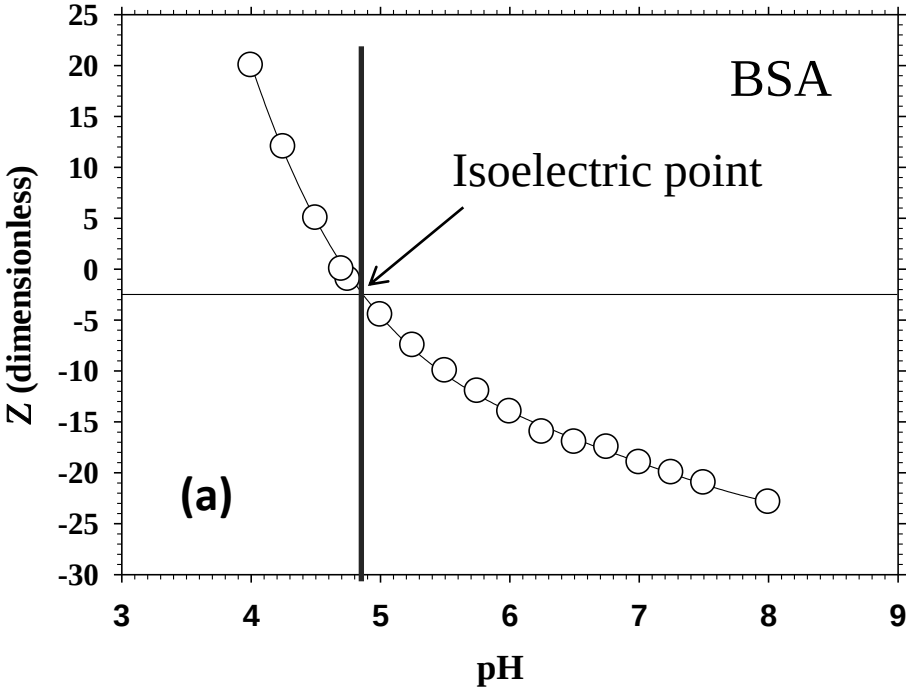

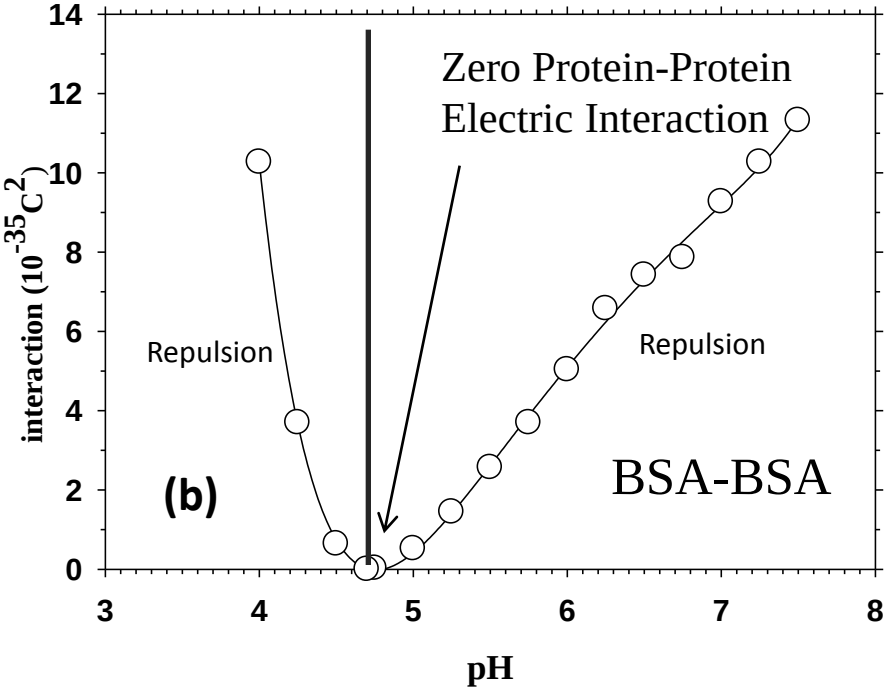

Figure 5.- The charge Z (a) and electrostatic interaction (b) values for BSA.

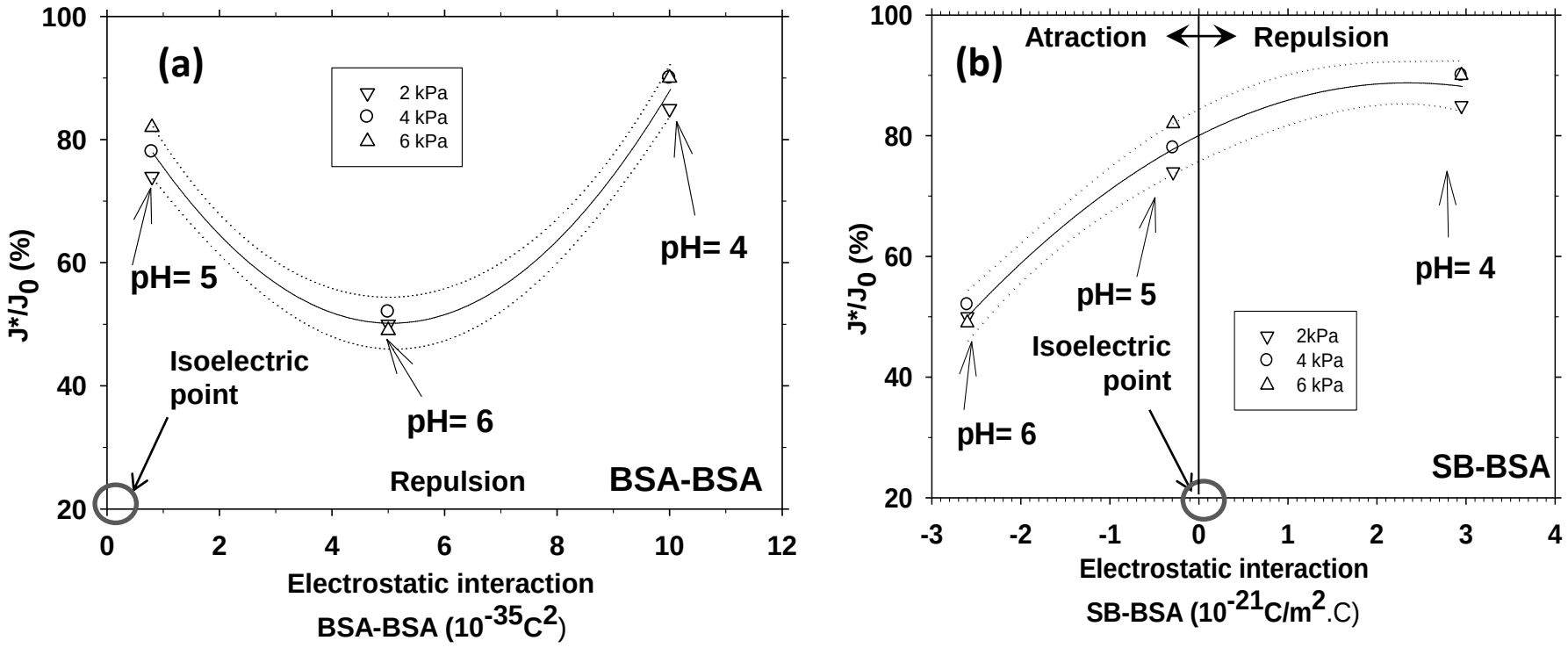

Figure 6.- The limit flux as a function of electrostatic interaction: (a) protein-protein and (b) membrane-protein.

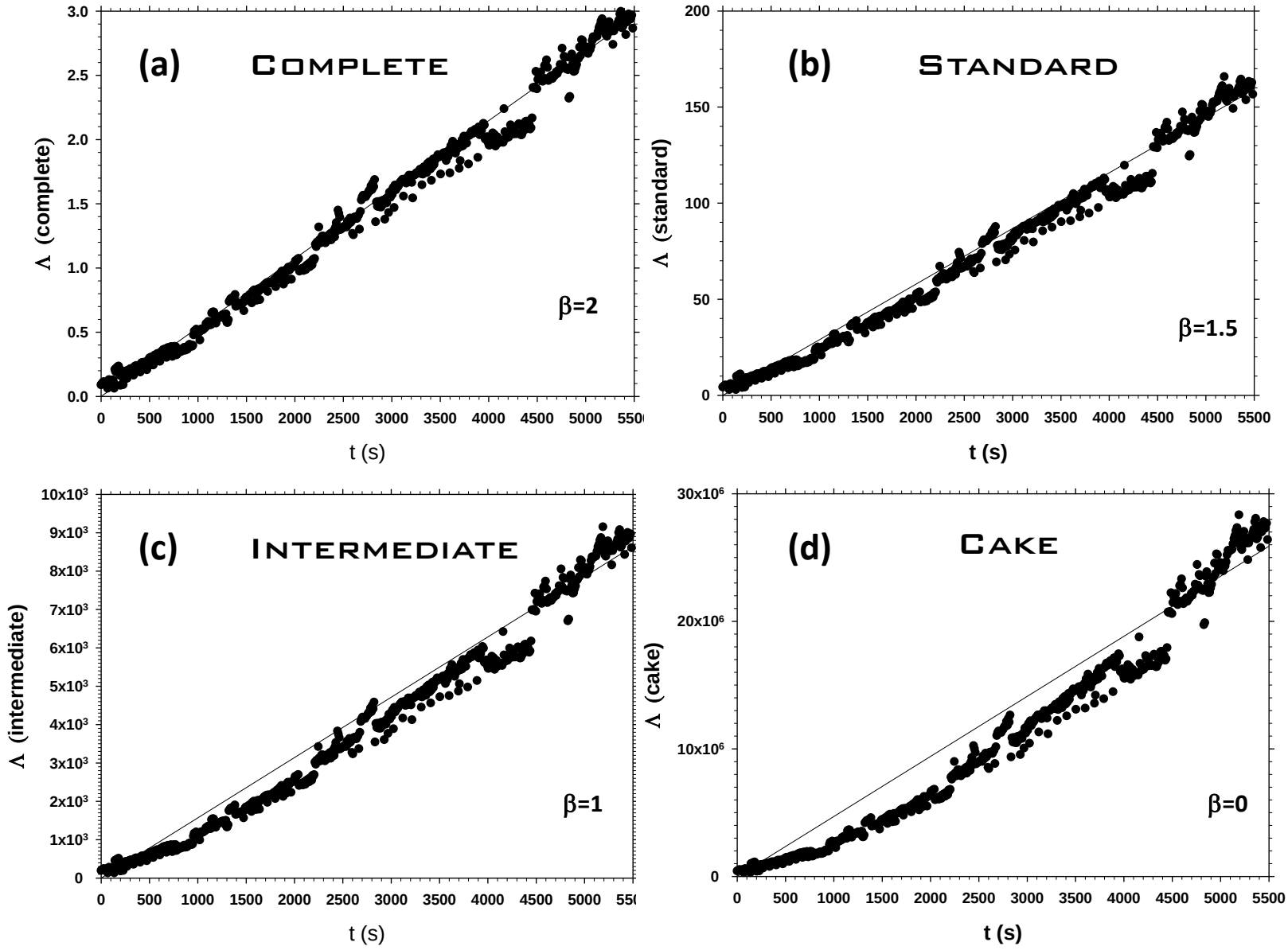

Figure 7.- The Λ coefficient for: (a) the complete fouling model; (b) the standard model; (c) the intermediate model and (d) the cake model. Data correspond to pH=6 and $\triangle$p= 4.85 KPa.

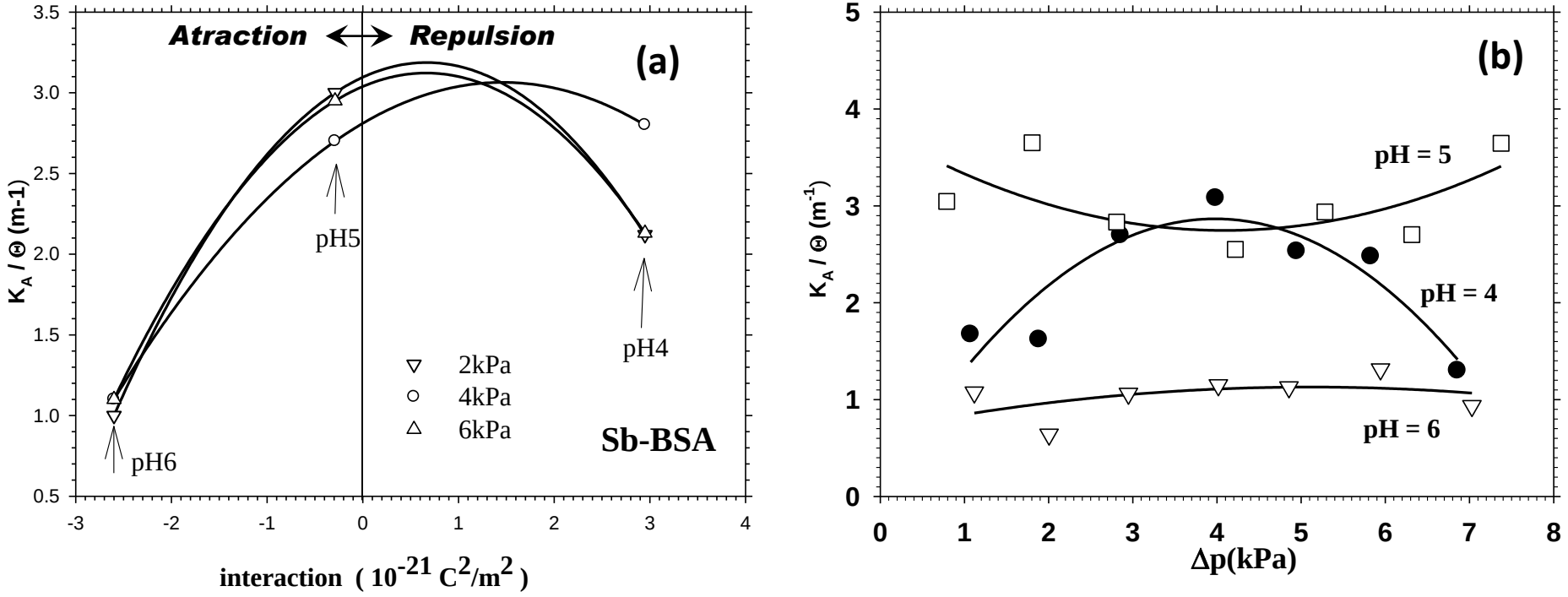

Figure 8.- The K_A /Θ kinetic constant as a function of: (a) the protein-membrane interaction and (b) the applied pressure, for the pH studied.